

Temperature uniformity, air flow and fuel efficiency in a 45ft reefer container

Climate chamber tests on 45ft intermodal refrigerated container PVDU385011[6]

L. J. S. Lukasse, M. G. Staal, J. Wildschut

CONFIDENTIAL

Temperature uniformity, air flow and fuel efficiency in a 45ft reefer container

Climate chamber tests on 45ft intermodal refrigerated container PVDU385011[6]

Authors: L. J. S. Lukasse, M. G. Staal, J. Wildschut

Institute: Wageningen Food & Biobased Research

This study was carried out by Wageningen Food & Biobased Research, subsidised by TKI Horticulture (the Dutch Ministry of Agriculture, Nature and Food Quality) under TKI number TU18098, funded by commissioners and commissioned by Anthos, H. Essers, Unit45 and Thermo King.

Wageningen Food & Biobased Research
Wageningen, September 2021

Confidential until August 2023

Report 2179

WFBR Project number: 6234166203

Version: Final

Reviewer: Erik Esveld

Approved by: Nicole Koenderink

Subsidized by: TKI Horticulture (the Dutch Ministry of Agriculture, Nature and Food Quality) under TKI number TU18098

Funded by: commissioners

Commissioned by: Anthos, H. Essers, Unit45 and Thermo King

Confidentiality of the report: Confidential until August 2023

© 2021 Wageningen Food & Biobased Research, institute within the legal entity Stichting Wageningen Research.

Confidential report. The research that is documented in this report was conducted in an objective way by researchers who act impartial with respect to the client(s) and sponsor(s). Nothing from this publication may be reproduced and/or made public without prior written permission by the director of Wageningen Food & Biobased Research. This report can be downloaded for free from August 2023 at <https://doi.org/10.18174/555537/> or at www.wur.eu/wfbr (under publications).

PO box 17, 6700 AA Wageningen, The Netherlands, T + 31 (0)317 48 00 84, E info.wfbr@wur.nl, www.wur.eu/wfbr.

All rights reserved. No part of this publication may be reproduced, stored in a retrieval system of any nature, or transmitted, in any form or by any means, electronic, mechanical, photocopying, recording or otherwise, without the prior permission of the publisher. The publisher does not accept any liability for inaccuracies in this report.

Contents

	Summary	5
1	Introduction	6
1.1	Aim	6
2	Theory (Key Performance Indicators)	7
3	Equipment specifications	9
3.1	Reefer container	9
3.1.1	Insulated body	9
3.1.2	Return air duct (bulkhead)	10
3.1.3	Supply air duct	11
3.1.4	Refrigeration unit type and settings	13
3.2	Dummy load during testing	14
3.3	Logger and sensor types	15
4	Test program	19
4.1	K-value + IR photos	19
4.2	Supply air flow rate	19
4.3	Choice for usage of air chute	20
4.4	Mapping of temperature, air velocity and static pressure difference	20
4.4.1	Tested configurations	20
4.4.2	Sensor positions	20
4.4.3	Temperature mapping tests	22
4.5	Fuel consumption and power uptake	24
5	Results	25
5.1	Measured K-value + IR photos	25
5.1.1	Measuring results	25
5.2	Supply air flow rate	26
5.3	Air velocities and static pressure differences	28
5.4	Temperature mapping	31
5.5	Fuel consumption and power uptake	33
6	Discussion	36
6.1	K-value + IR photos	36
6.2	Supply air flow rate	36
6.3	Air velocities and static pressure differences	38
6.4	Temperature mapping	40
6.4.1	General temperature distribution patterns	40
6.4.2	Maximal cargo temperature difference ΔT_{cargo}	40
6.4.3	ΔT_{cargo} in heating mode vs. cooling mode.	40
6.4.4	Effect of evaporator fan speed	41
6.4.5	Air flow distribution	41
6.4.6	Return air temperature control	41
6.4.7	Effect of 24 or 26 pallets	42
6.4.8	Effect of run mode	42
6.5	Fuel consumption and power uptake	43
6.5.1	Global fuel efficiency and COP	43
6.5.2	Cycle-sentry mode	43

6.5.3	Heating mode efficiency	43
6.5.4	Effect of evaporator fan speed setting	43
6.5.5	Effect of heat load	43
6.5.6	Options to improve energy efficiency	43
6.6	Temperature uniformity requirements and feasibility	44
6.6.1	Feasible of the three equipment requirements	45
6.7	Comparison to other tested containers	45
7	Conclusions	49
8	Recommendations	50
	Literature	51
	Acknowledgements	52
Annex 1	Temperature graphs	53
Annex 2	steady state temperatures in 3D	61
Annex 3	Test log	67

Summary

Project partners Essers, Thermo King and unit45 have developed a new type of 45ft reefer container. In a series of climate chamber tests the following parameters are measured and evaluated for one specimen of this container type: K-value, fuel efficiency, air flow rate, distribution of air flow, static air pressure distribution, and temperature distribution in extreme ambient temperatures. The steady state temperature distribution has been measured in 22 test variations: loaded with 26 or 24 pallets, different extreme summer and winter temperatures and with various unit settings. In these test a dense grid with more than 50 internal temperature loggers was used, which allows a 3D comparison of temperature distribution in the different conditions.

Important is the temperature uniformity requirement: for long-distance carriage of lily bulbs, the difference between the warmest and the coldest cargo temperature shall never be more than 3°C. The most important conclusion is that temperature differences inside the container are too large, especially in cooling mode. In cooling mode at $T_{\text{set}} = 4^{\circ}\text{C}$ and $T_{\text{amb}} = 40^{\circ}\text{C}$ the best achieved difference between the warmest and the coldest cargo temperature is 5.3°C (ΔT_{cargo}), even when the load is reduced from 26 to 24 pallets. This ΔT_{cargo} of 5.3°C is 2.4°C smaller than in the earlier tested reference 45ft rail container and comparable to ΔT_{cargo} in the earlier tested 40ft marine container loaded with 21 pallets.

In the discussion (chapter 6) the impact of the K-value, the supply air duct, and the return air duct on the container performance is analysed. In chapter 8, a detailed list of concrete recommendations is provided for Thermo King, Unit45 and Essers on how to improve the performance of this container. It is expected that improving the insulation (K-value), better air distribution towards the door-end (supply air duct) and removal of air flow bottle necks in the return air duct may suffice to achieve ΔT_{cargo} comparable to ΔT_{cargo} in a 40ft marine container loaded with 20 pallets and meet the temperature uniformity requirement, possibly even in a load of 26 pallets.

For additional information about this report, see the colophon.

1 Introduction

Project partners Essers, Thermo King and unit45 have developed a new type of 45ft reefer container. A purpose of the development is that the new 45ft reefer container should have a reduced energy consumption and should be suited for the long-distance carriage of lily bulbs. In that case it is required that the difference between the warmest and the coldest steady state cargo temperature is never more than 3°C.

Key performance indicators of refrigerated transport equipment are K-value of the container, fuel efficiency and cargo temperature distribution under extreme ambient temperatures. In a series of climate chamber tests these KPIs are measured and evaluated for one specimen of the new 45ft container type.

The cargo temperature distribution inside reefers directly relates to air flow distribution. Therefore also the unit's air flow rate, distribution of air flow, and static air pressure distribution inside the container are measured.

The air and temperature distribution is affected by a number of parameters, amongst which: difference between internal and external temperature, air flow rate of the unit's evaporator fans, and cargo stowage pattern. Therefore the following factors were varied in the tests: 1) Internal and external temperature settings T_{set} / T_{amb} , 2) unit's run mode, 3) unit's method of drive, 4) evaporator fan speed, 5) cargo stowage.

1.1 Aim

The tests have multiple purposes:

1. Assess K-value
2. To measure energy efficiency, steady state temperature distribution, pull down and pull up curves in extreme ambient temperatures.
3. To quantify the effect of T_{set} / T_{amb} , run mode, method of drive, evaporator fan speed, and some cargo stowage variations on temperature distribution in 45ft reefer containers.
4. To collect data suitable for CFD model calibration afterwards.
5. Compare this container's temperature uniformity to an earlier tested reference 45ft container and to an earlier tested 40ft container.

2 Theory (Key Performance Indicators)

In an experimental study on temperature distribution in reefer containers lots of data need to be evaluated. The three typical stages of interest are: steady state, power off, and pulldown. In an experiment a natural procedure is to first prepare for pulldown by establishing steady state at initial temperature (stage 0), then pulldown (stage 1) to steady state (stage 2), then introduce a power off period of a predefined duration (stage 3), and then recover the temperatures (stage 4) to steady state again (stage 2). Figure 1 shows an arbitrary example (note: recovery stage missing from this illustration). The 'temperature recovery' stage has similarities with the initial pulldown stage after hot-stuffing. The difference is that at the start of a recovery period there are typical temperature gradients in the cargo from warm side temperatures to a colder core, while at the start of an initial pulldown stage all cargo temperatures are approximately equal.

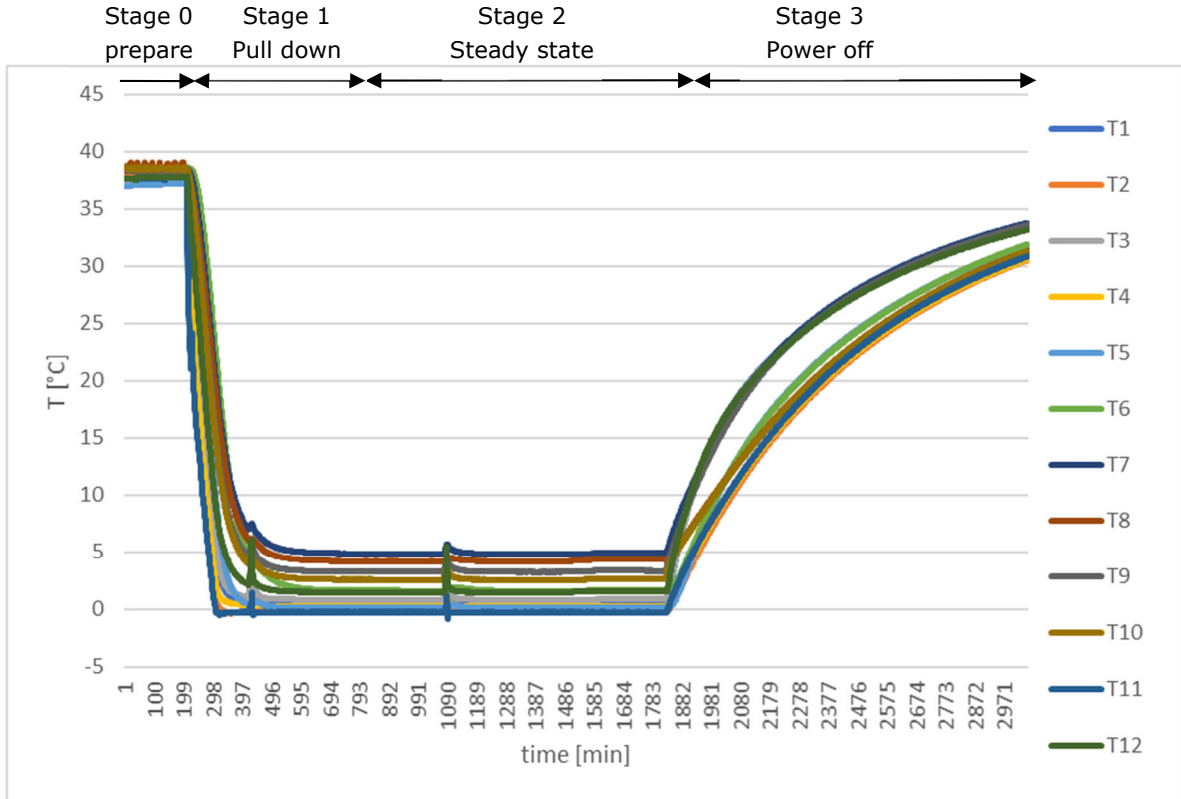


Figure 1 example of temperatures recorded during four consecutive test stages. Series T1 till T12 show temperatures recorded by temperature sensors placed at different positions in cargo.

To condense the information contained in the temperature readings to one, or a few, informative numbers, this report uses the key performance indicators listed in Table 1.

The maximal cargo temperature range is the measure for the cargo temperature uniformity:

$$\Delta T_{cargo} = T_{warmest} - T_{coldest} \quad [^{\circ}\text{C}] \quad (1)$$

where

$T_{warmest}$ = warmest time-averaged cargo temperature sensor during steady state

$T_{coldest}$ = coldest time-averaged cargo temperature sensor during steady state

Note that in this report cargo temperature is defined as temperature measured by a temperature sensor taped to the dummy load of cartons. Under ideal air distribution conditions ΔT_{cargo} is the same as the absolute value of the temperature difference between the unit's return and supply air temperature, defined as ΔT_{unit} :

$$\Delta T_{unit} = |T_{ret} - T_{sup}| \quad [^{\circ}\text{C}] \quad (2)$$

where

T_{ret} = refrigeration unit's time-averaged return air temperature during steady state

T_{sup} = refrigeration unit's time-averaged supply air temperature during steady state
 The quality of the air flow distribution in a steady state is scored with a dimensionless ratio, called Temperature Distribution Factor TDF:

$$TDF = \frac{\Delta T_{cargo}}{\Delta T_{unit}} = \frac{T_{warmest} - T_{coldest}}{|T_{ret} - T_{sup}|} \quad [-] \quad (3)$$

In case of ideal air flow distribution $\Delta T_{cargo} = \Delta T_{unit}$, resulting in $TDF = 1$. In practice the air flow distribution is usually non-ideal, and the maximal temperature range ΔT_{cargo} in the reefer is larger than ΔT_{unit} , resulting in $TDF > 1$. The worse the temperature uniformity the bigger ΔT_{cargo} , and the ratio TDF increases linearly with ΔT_{cargo} .

Table 1 **key performance indicators used for different variables in the tests**

variable	key performance indicator (KPI)
Temperature uniformity	ΔT_{cargo} , warmest time-averaged cargo temperature minus coldest time-averaged cargo temperature during steady state.
Air flow distribution	Ratio TDF (eqn. 3) during steady state.
Pull down/up	Just visual presentation of temperature graphs
power off	Just visual presentation of temperature graphs
Door opening	Just visual presentation of temperature graphs
recovery	Just visual presentation of temperature graphs

3 Equipment specifications

3.1 Reefer container

Container identification number	PVDU385011[6]
Tare weight	6,300 kg
Max. gross weight	34,000 kg

3.1.1 Insulated body

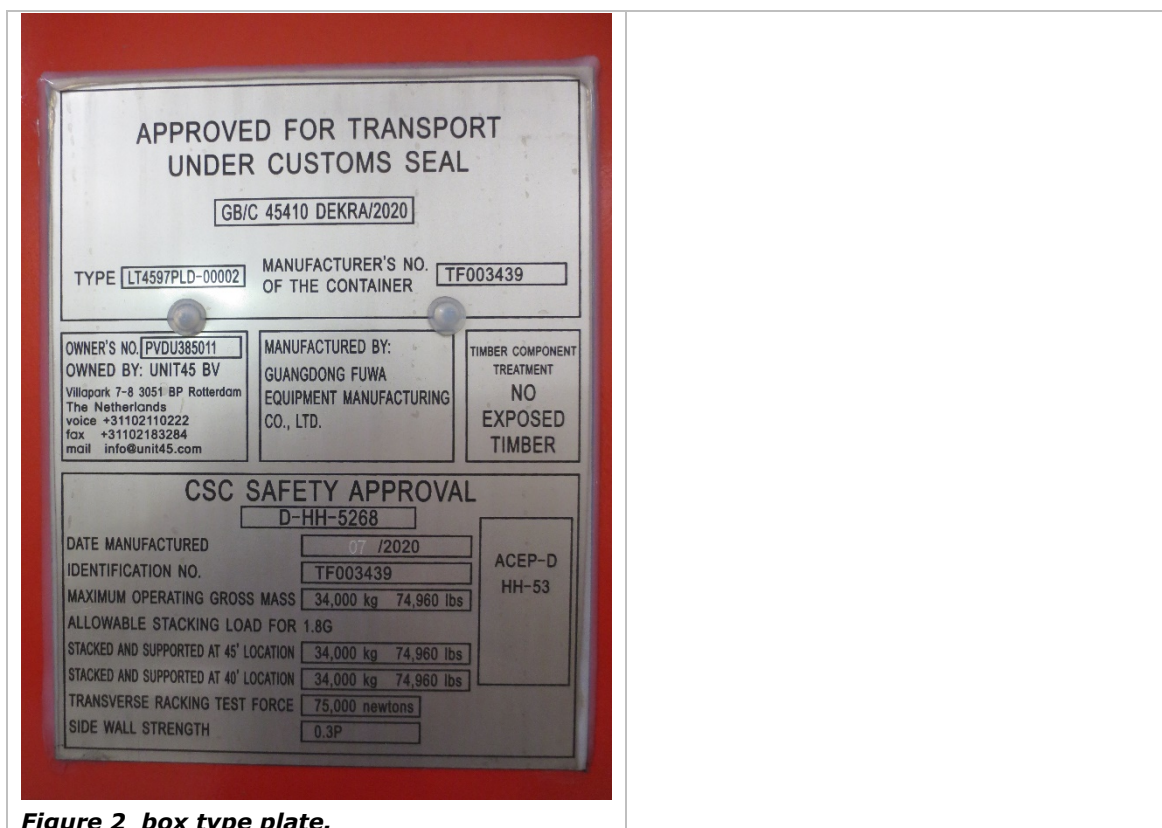


Figure 2 box type plate.

Description	Value
Container box identification number	TF003439
Manufacturing date	07/2020
Box manufacturer	Guangdong Fuwa Equipment Manufacturing Co. Ltd.
Box type	LT4597PLD-00002
External dimension of insulated enclosure	LxWxH = 13.46 x 2.59 x 2.81 m
Inside dimensions of insulated enclosure	L(@floor, without return air duct)xWxH = 13.31 x 2.45 x 2.60 m
Thickness of doors	40 mm in thin areas, 65 mm in thick areas. The thick areas cover ± 40% of the doors.
Thickness of walls	70 mm
Thickness of roof	95 mm
Thickness of floor	115 mm
Thickness of front wall (calculated)	110 mm (not measured, calculated as $L_{\text{extern}} - L_{\text{intern}} - \text{door thickness}$)

Gooseneck dimensions (position, L, W, recess)	@ unit-end in center of container, L = 3.88 m, W = 1.03 m, recess = 4.5 cm (i.e. in this area the floor is 4.5 cm thinner than in rest of floor)
Supply air outlet (grid)	W x H = 58 x 18 cm
Distance between top of supply air outlet and ceiling	10 cm
Distance between supply air outlet and front wall	0 cm

Table 2 *calculated surface areas and internal volume.*

Description	value
Total floor area	32.61 m ²
Usable internal volume	84.78 m ³
Total internal surface area S _i of body	147.17 m ²
Total external surface area S _e of body	159.92 m ²
Mean surface are $S = \sqrt{S_i \times S_e}$	153.41 m ²

3.1.2 Return air duct (bulkhead)

Description	Value
Return air duct width @ bottom	222 cm
Return air duct width @ top	170 cm
Distance floor – lower end of return air duct	13 cm
Space between front wall and bulkhead, i.e. depth of return air duct	4.5 cm
Top of return air duct	Open / closed
Unit's return air grid (W x H)	132 x 48 cm

Figure 3 shows a photo of the return air duct. Behind the brownish wooden panel is the unit's return air grid (Figure 4). Underneath the wooden panel is the bulkhead, a.k.a. as front stop panel, which is a metal plate of only 3 mm thickness. Mounted on the floor are the pallet stoppers. The container was delivered for testing without the wooden panel, but Thermo King representatives installed the panel before start of the first test, and it has stayed in place during all tests.



Figure 3 *bulkhead / return air duct during testing.*



Figure 4 *unit's return air grid.*



Figure 5 bulkhead / return air duct as it arrived.



Figure 6 top view of return air duct between bulkhead and front wall.

3.1.3 Supply air duct

The supply air duct, a.k.a. as air chute, has a complex geometry. See the photos in Figure 7 - Figure 10 for an impression.



Figure 7 container's supply air duct and supply air grid.



Figure 8 container's supply air duct.



Figure 9 container's supply air duct.



Figure 10 container's supply air duct (top of photo).

Table 3 and Table 4 specify the measured dimensions of the supply air duct.

Table 3 dimensions of supply air duct.

Description	Value
Length of supply air duct	10.26 m
Height of opening at end of supply air duct	1.5 cm at sides, 2.5 cm in center
Width of opening at end of supply air duct	1.42 m

The dimensions in Table 4 relate to the sketch in Figure 11. In Table 4 h_{min} is the distance between container floor and the lowest point of the air chute, h_0 is the height of the opening between ceiling and air chute, and w is the distance between the wall and the air chute.

Does the shape of the supply air duct change when the evaporator fans start to run due to the positive air pressure above the air chute? We measured it, and we observed that even in the first meters from the unit-end the air chute position changes less than a cm. Therefore this effect can safely be deemed negligible.

Table 4 dimensions of supply air duct (see Figure 11 for meaning of h_{min} , h_0 and w).

Distance from unit-end [m]	h_{min} [m]	h_0 [cm]	w [cm]
0	2.21	36	52
1	2.35	16	53
2	2.44	8	52
3	2.49	5	52
4	2.52	3.5	52
5	2.53	3	52
6	2.54	2.5	52
8	2.56	2	52
9.5	2.57	2	52
10 (end)	2.58	1.5	52

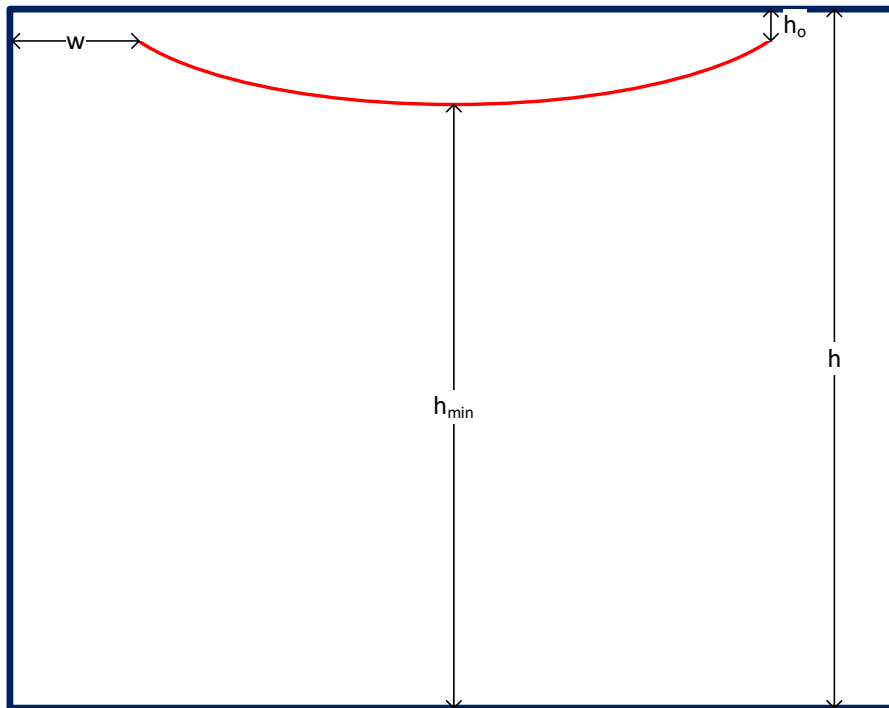


Figure 11 sketch of transversal cross-section of supply air duct (red) in container (blue).

As visible in Figure 9 the air chute contains 9 holes of Ø12 cm diameter. The position of the holes is: 3 next to each other in transversal direction, at 330, 450 and 570 cm from the unit-end. In initial smoke tests it was observed that very little air flows through these holes.

3.1.4 Refrigeration unit type and settings

Description	Value
Manufacturer	Thermo King
Type	Advancer A-500
Serial no.	GLW1253687
Manufacturing date	2020
Controller's software revision	4.0.0.2
Date of last PTI	Unknown
Defrost interval	Setting not available



Figure 12 Thermo King unit type plate.

3.2 Dummy load during testing

During tests on air flow distribution, static pressure distribution and temperature distribution the container was filled with a dummy load. The dummy load consisted of empty palletized pallet boxes. Table 5 lists all relevant parameters of the pallets and boxes.

Table 5 *dummy load parameters.*

Description	Value
Dimensions of pallets	L x W x H = 120 x 100 x 16 cm
Weight of pallet	18.9 kg
Area of openings at 120 cm side of pallet	2 openings of 41.7 x 9.5 cm (= 396 cm ²)
Area of openings at 100 cm side of pallet	2 openings of 38.5 x 11.5 cm (=443 cm ²)
No. of slats on top of pallet	10 slats of approx. 8 cm wide
Distance between slats on top of pallet	6 openings of approx. 7 cm
All slat distances ± equal?	No, see Figure 13 and Figure 14.
Size of pallet boxes	L x W x H = 118.5 x 98.5 x 87.0 cm
Weight of one pallet box	6.0 kg
No. of pallet box layers	2.5 (see Figure 15)
Height of pallet stacked with 2.5 tiers of pallet boxes	233 cm

The pallet boxes were specially purchased for this test from webshop.viv.nl/palletdozen-voor-blokpallet-dubbelgolf-1185-x-985-x-870-mm.



Figure 13 *pallet used for the experiment.*



Figure 14 *bottom view of the pallet*



Figure 15 2.5 boxes stacked on top of each pallet.



Figure 16 sensors mounted on the pallet box.

3.3 Logger and sensor types

This section briefly describes all measurement devices used during the tests.

Table 6 used logger types.

Logger type	number	measured parameter
ATP sensors	16	T [°C]
LogTags (Figure 19)	46	T [°C]
Air pressure difference sensor	1	Pressure difference [Pa]
Hot wire anemometers, type EE65-VB5, range 0.2 till 20 m/s, log every 15 sec	12	Air velocity [m/s]
Hot wire anemometers, type EE576-V3B2, range 0.2 till 2 m/s, log every 15 sec	6	Air velocity [m/s]
Hot wire anemometers, type EE671, range 0.2 till 10 m/s, log every 30 sec, wireless.	16	Air velocity [m/s]

Hot wire anemometers type EE671 record till their batteries are flat, at the set log interval of 30 s. The batteries last approximately 5 hours. The two other types of hot wire anemometers are powered by the grid (230 V / 50 Hz).

Accuracy of hot wire anemometer EE65-VB5: $\pm (0.2 \text{ m/s} + 3\% \text{ of measured value})$

Accuracy of hot wire anemometer EE576-V3B2: $\pm (0.08 \text{ m/s} + 4\% \text{ of measured value})$

Accuracy of hot wire anemometer EE671: $\pm (0.3 \text{ m/s} + 4\% \text{ of measured value})$



Figure 17 hot wire anemometers EE576-V3B2 (left) and EE65-VB5 (right).



Figure 18 EE671 hot wire anemometer.



Figure 19 LogTag logger for temperature.



Figure 20 ATP sensor (= 4-wire PT100 temperature sensors of IEC751 class A, manufacturer: Tempcontrol).

Accuracy of all temperature sensors: $\pm 0.5^{\circ}\text{C}$

The log interval during the tests is 5 min. for the LogTags and 1 min. for the ATP sensors. Only the readings of the ATP temperature sensors are real-time available.



Figure 21 ZES TM396 power meter used to record the unit's power uptake.



Figure 22 testo 480 pressure difference sensor

Accuracy of the unit's power uptake sensor: $\pm 0.5\%$

Accuracy of testo 480 pressure difference sensor: $\pm (0.3 \text{ Pa} + 1\% \text{ of measurement value})$

For assessing the supply air flow rate a handheld hot wire anemometer (testo 425) is used (Figure 23, Figure 24). Accuracy of testo 425: $\pm (0.03 \text{ m/s} + 5\% \text{ of measurement value})$ in the range of 0 till 20 m/s.



Figure 23 handheld hot wire anemometer used to assess supply air flow rate.



Figure 24 close-up of hot wire sensor.

The unit's diesel consumption is measured by placing its fuel lines in a large drum placed on a scale, in an insulated box to avoid flocculation of the diesel during -20°C chamber temperatures (Figure 25). The weight of that drum is logged at a 1 minute interval. The scale is a Mettler Toledo PBA330-BC150B with reproducibility 25 g, See Figure 25 for a photo.



Figure 25 diesel drum on scale in insulated box.

4 Test program

4.1 K-value + IR photos

The K-value of the empty container was measured according to ATP procedures (ATP, 2020) by following the relevant steps in WFBR internal Standard Operating Procedure T-10006. In the ATP test conditions ($T_{\text{outside}} = 7.5^{\circ}\text{C}$ and $T_{\text{inside}} = 32.5^{\circ}\text{C}$) infrared photos of the container doors were made on request of Essers to check for thermal bridges.

4.2 Supply air flow rate

The supply air flow rate was measured after completion of all other tests. The measurements were done in an empty container. The procedure was to measure the air velocity [m/s] averaged over the supply air grid and multiply it by the area [m²] of the supply air grid. First the supply air duct was removed. Then the air velocity right in front of the supply air grid was measured as an average over time and place. The average was assessed with the handheld anemometer's time-averaging function while slowly moving the handheld anemometer over the complete supply air grid for a period of 40 till 60 seconds (Figure 26). That time- and space-averaged measurement was repeated twice. If the mutual difference was more than 10% a third repetition was done after which the deviant measurement was discarded. The measurement was performed for a number of different combinations of method of drive, set evaporator fan speed, and position of the wooden panel (Figure 3) in front of the return air grid (Figure 4). For each combination the unit was started at a setpoint close to the actual T_{ret} , which was always around 20°C. The reason to set T_{set} to T_{ret} was that the impression arose that the unit increased its evaporator fan speed when the difference between T_{set} and T_{ret} was large. All tests were done within in a time frame of two hours.

This test procedure is less accurate than for example the test procedure described in ISO5801, but it is convenient and fast, and therefore adequate for roughly checking manufacturer specs and mutually comparing different situations.



Figure 26 measurement of average supply air velocity.

4.3 Choice for usage of air chute

Before the container arrived for testing Alain van Schaik (Thermo King) had informed parties that Thermo King might be able to install a so-called air straightener as a good alternative for the air chute. On 28-10-2020, five days after the container arrived in Wageningen, Mark Vermeulen (Thermo King) and Wil van de Wouw (Thermo King) visited Wageningen. They then explained that there is no air straightener available for this unit. Together with Marcel Staal (WFBR), Wil and Mark performed smoke tests to visualize the air flow in the empty container with and without air duct. Based on their visual observation, caught on video, the three unanimously concluded that the air chute was needed to facilitate sufficient air flow towards the door-end.

4.4 Mapping of temperature, air velocity and static pressure difference

4.4.1 Tested configurations

The following configurations are tested:

1. Configuration 1 (reference): standard container with standard stowage of 26 pallets and air chute
2. Configuration 2 (test): deviation from reference: 24 pallets

Figure 27 till Figure 28 visualize the defined configurations.

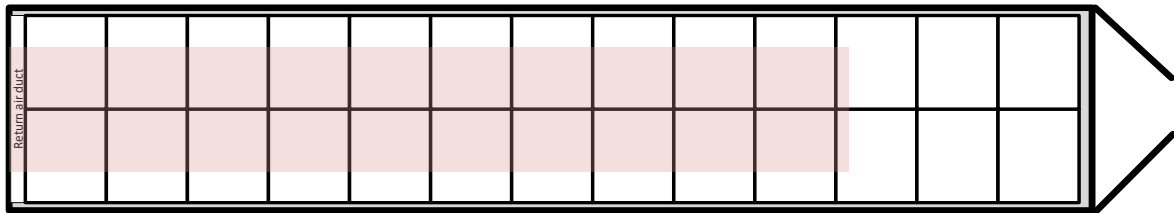


Figure 27 configuration 1: reference (top view), in red the air chute.

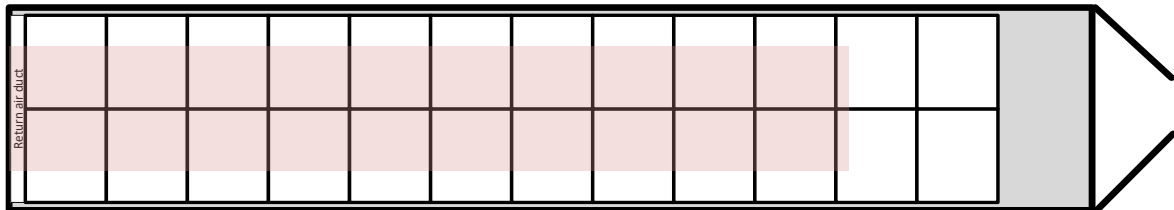


Figure 28 configuration 2: test (deviation from reference: 24 pallets), in red the air chute.

Table 7 (measured) stowage parameters.

Description	Value
Distance between last pallet and door (in case of 26 pallets load)	15 cm
Height of headspace (= distance between ceiling and top of cargo)	27 cm
Air flow blocking at door-end	none

In a climate chamber at WFBR the above listed configurations were subjected to a series of test conditions. In nearly each test condition the objective is to gain insight in energy consumption, either electric power uptake or diesel consumption, and distribution of temperature and air flow.

4.4.2 Sensor positions

Figure 29 and Figure 30 schematically depict the sensor locations for the reference configuration 1. The pallets in Figure 29 are numbered 1 till 26 in the order in which they are placed in the container. The 3 yellow dots indicate LogTag sensors outside the container: one at the air inlet to the condenser,

and two at 10 cm from the container walls at the centre of both sides. The 2 yellow squares indicate 2 inside ATP sensors in pallets 4 and 22, these are placed inside the box at half height, and used to verify if inside temperatures have reached steady state. All LogTag temperature recorders are taped at the outside to the front or rear of boxes. Where applicable the recorder's sensor faces, but does not touch, the wall. Wherever there is red square, there are three LogTag positions above each other: at the bottom, middle and upper corner of the pallet load. The red and orange dots at the unit-end indicate positions of LogTags respectively ATP sensors, both at the inlet of the return air duct (taped to the inside of return air duct at its lower-end) and in supply air (tie-wrapped to the supply air grid). The orange squares indicate the position of the internal ATP sensors. Figure 29 contains numbers adjacent to each temperature sensor position. These numbers are the unique serial numbers of the sensors, where the upper number is physically the upper sensor (e.g. at the door-end pallet 25 contains ATP sensor number ATP9 at the top and ATP10 at the bottom). The side view in Figure 30 especially helps to visualize the measurement locations for air velocity and pressure. Dark green dots indicate the positions for measurement of static pressure difference compared to the position of the purple dot: 0, 2, 4, 6, 8, 10, and 12 m from unit-end. Blue dots indicate the hot wire anemometer positions during measurement in the center of pallet openings: 0, 1, 2, 3, 4, 5, 6, 7, 8, 9, 10, 11 and 12 m from unit-end. Blue triangles indicate the hot wire anemometer positions above the cargo: halfway between air chute and ceiling.

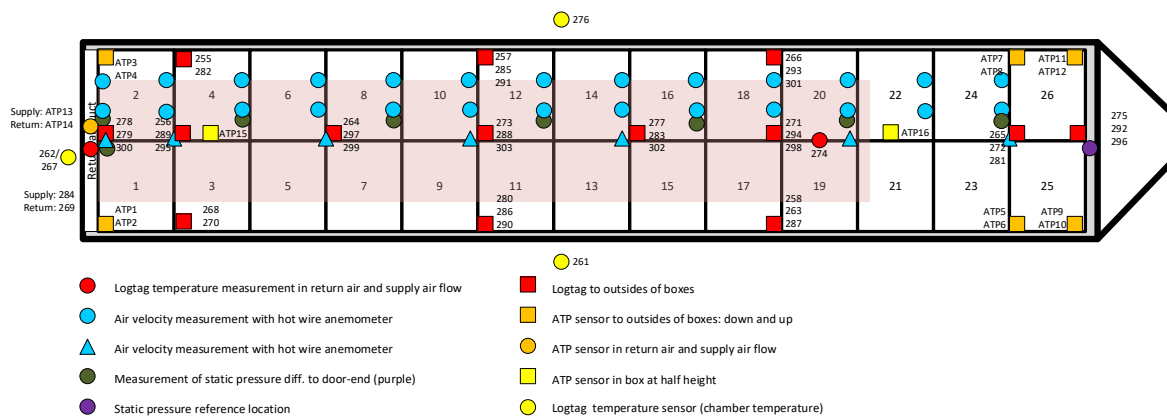


Figure 29 schematic representation of sensor positions in configuration 1 (top view).

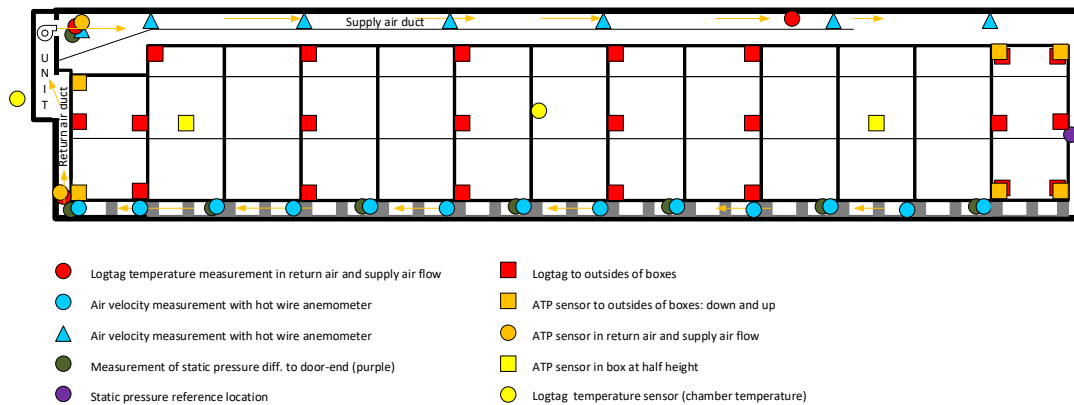


Figure 30 schematic representation of sensor positions in configuration 1 (side view).

Figure 31 and Figure 32 visualize the sensor locations during configuration 2. After the preceding paragraph these figures need no further explanation.



Figure 31 schematic representation of sensor positions in configuration 2 (top view).

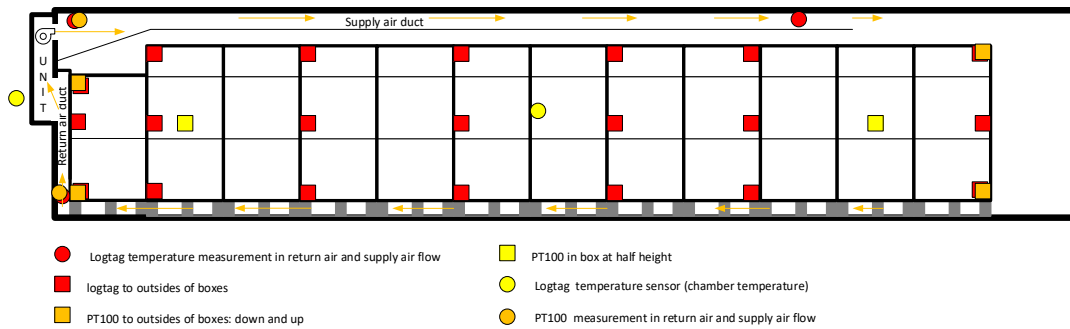


Figure 32 schematic representation of sensor positions in configuration 2 (side view).

4.4.3 Temperature mapping tests

Table 8 till Table 10 list all conducted temperature mapping tests. The first column in each of these tables lists the unit's temperature setpoint T_{set} and the intended chamber temperature T_{amb} as measured by the two sensors at 10 cm from the container walls at the center of both sides (yellow dots in Figure 29 till Figure 32). Column 2 is the test number assigned to each test. The numbering was chronologically in the plan upfront. For many practical reasons the eventual work order deviated from the original plan. To avoid confusion in the data processing the original numbering has been kept in the report. Column 3 lists the run mode, as on virtually every trailer refrigeration unit there are two possible values: continuous or cycle-sentry. Column 4 lists the method of drive: diesel or electric (50 Hz / 400 V). Column 5 lists the set evaporator fan speed, where the unit's controller allows three possible settings: high, standard, or maximum. The last column lists the number of pallets: 26 in case of reference configuration 1 (Figure 27), or 24 in case of test configuration 2 (Figure 28).

As seen in Table 8 till Table 10 tests are performed at multiple combinations of T_{set} / T_{amb} . These test conditions were chosen in consultation with Essers. There is a rough categorization in two ranges for set temperature T_{set} and three ranges for ambient temperature T_{amb} . The chosen T_{set} is in the ranges typical for pharmaceuticals in either the chilled segment (2 till 8°C) or the ambient segment (15 till 25°C). The chosen T_{amb} is typical of winter tests ($T_{amb} = -22^\circ\text{C}$), summer tests ($T_{amb} \geq 35^\circ\text{C}$), and some midseason tests ($T_{amb} = 20^\circ\text{C}$). The summer tests are further diversified in mild and extreme conditions. These test conditions serve this report's purposes and are useful to Essers for other reasons.

Table 8 steady state tests in test programme.

T_{set} / T_{amb} [°C]	test no.	Run mode	Method of drive	Evap fan speed	# pallets
6 / -22°C	6	Continuous	Electric	HIGH	26
6 / -22°C	7	Continuous	Electric	standard	26
6 / -22°C	8	Continuous	Diesel	HIGH	26
22 / -22°C	10	Continuous	Electric	HIGH	26
22 / -22°C	10B	Continuous	Electric	STANDARD	26
20 / -22°C	11	Continuous	Electric	HIGH	26

20 / -22°C	12	Continuous	Diesel	HIGH	26
20 / -22°C	17	Cycle-Sentry	Electric	HIGH	26
20 / -22°C	18	Cycle-Sentry	Diesel	HIGH	26
20 / 20°C	19	Cycle-Sentry	Diesel	HIGH	24
20 / 20°C	20	Cycle-Sentry	Electric	HIGH	24
20 / 20°C	21	Continuous	Diesel	HIGH	24
20 / 20°C	22	Continuous	Diesel	STANDARD	24
20 / 20°C	23	Cycle-Sentry	Diesel	STANDARD	24
20 / 40°C	25	Cycle-Sentry	Diesel	HIGH	24
18 / 40°C	26	Continuous	Electric	HIGH	26
20 / 37°C	26A	Continuous	Electric	HIGH	24
20 / 40°C	26B	Continuous	Electric	HIGH	24
20 / 40°C	27	Continuous	Diesel	HIGH	24
4 / 35°C	31	Continuous	Electric	HIGH	26
4 / 40°C	33	Continuous	Diesel	HIGH	26
4 / 40°C	33A	Continuous	Diesel	MAX	26
4 / 40°C	33B	Continuous	Diesel	MAX	24
5 / 40°C	33C	Continuous	Diesel	MAX	24
4 / 40°C	33D	Continuous	Diesel	MAX	24
4 / 40°C	39	Cycle-Sentry	Diesel	STANDARD	24
4 / 40°C	40	Continuous	Diesel	STANDARD	24

Table 9 pull down and pull up tests in test programme.

T_{set} / T_{amb} [°C]	test no.	Run mode	Method of drive	Evap fan speed	# pallets
6 / -22°C	5	Continuous	Electric	HIGH	26
4 / 45°C	30	Continuous	Electric	HIGH	26

Table 10 contains a 7th column that briefly describes the purpose of that test. E.g. test 13 is a 4 hours power of test: just record how temperatures evolve after powering the unit off in steady state at T_{set} / T_{amb} . Test 14 is the recovery test, initiated directly after test 13 with the purpose to record how temperatures recover after a 4 hours power off period. Every recovery test in Table 10 directly follows the test mentioned in the row above. One test in Table 10 is a manual defrost + recovery test: how does a manual defrost disturb temperatures and how do they recover after defrost termination?

Table 10 *power off/ door opening / defrost tests in test programme.*

T_{set} / T_{amb} [°C]	test no.	Run mode	Method of drive	Evap fan speed	# pallets	Description
20 / -22°C	13	N/A	OFF	N/A	26	4 h. power off
20 / -22°C	14	Continuous	Electric	HIGH	26	recovery
20 / -22°C	15	N/A	OFF	N/A	26	1 h. door opening
20 / -22°C	16	Continuous	Electric	HIGH	26	recovery
4 / 40°C	34	N/A	OFF	N/A	24	1 h. door opening
4 / 40°C	35	Continuous	Diesel	MAX	24	recovery
4 / 40°C	36	Continuous	Diesel	MAX	24	manual defrost + recovery
4 / 40°C	37	N/A	OFF	N/A	24	4 h. power off
4 / 40°C	38	Cycle-Sentry	Diesel	STANDARD	24	recovery

4.5 Fuel consumption and power uptake

Fuel consumption and power uptake have not been measured according to specification of ATP and/or EN16440 (EN16440, 2015). This was a deliberate choice to limit the costs of testing. Instead fuel consumption and power uptake were measured during the temperature mapping tests mentioned in section 4.4.

5 Results

5.1 Measured K-value + IR photos

This section reports the K-value measured according to ATP procedures. The duration of the test is a bit shorter than ATP requires, and the outside temperature fluctuates a bit more than ATP allows. Yet these deviation from the specifications have a negligible effect on the measurement result.

Testing method	:	inside heating
Start of inner heating (yyyy-mm-dd hh:mm:ss)	:	2020-12-09 14:15:58
Start time of steady state conditions (yyyy-mm-dd hh:mm:ss)	:	2020-12-09 19:00:58
End time of steady state conditions (yyyy-mm-dd hh:mm:ss)	:	2020-12-10 07:00:58
Total duration of test (hh:mm:ss)	:	16:45:00
Duration of steady state conditions (hh:mm:ss)	:	12:00:00

5.1.1 Measuring results

Outside

Mean outside temperature of body (θ_e)	:	7.31	°C
Max. difference between two mean outside temperatures	:	0.93	°C
Max. difference between two outside measurement locations	:	1.24	°C

Inside

Mean inside temperature of body (θ_i)	:	32.50	°C
Max. difference between two mean inside temperatures	:	0.07	°C
Max. difference between two inside measurement locations	:	1.40	°C

Mean temperature difference achieved ($\Delta\theta = \theta_i - \theta_e$)	:	25.19	°C
-------------------------------------------------------------------------------	---	-------	----

Mean temperature of walls of the body achieved ($\frac{\theta_e + \theta_i}{2}$)	:	19.91	°C
------------------------------------------------------------------------------------	---	-------	----

Electric power consumption (heaters + fans),	Q =	1877.61	W
----------------------------------------------	-----	---------	---

Total heat leakage rate ($Q/\Delta\theta$),	U =	74.54	W/°C
-----------------------------------------------	-----	-------	------

Total heat transfer coefficient $\left(K = \frac{Q}{\Delta\theta * S} \right)$,	K =	0.486	W.m ⁻² .°C ⁻¹
------------------------------------------------------------------------------------------	------------	-------	-------------------------------------

Max. error in measured K in this test,	:	±	5	%
----------------------------------------	---	---	---	---

The IR photos (Figure 33, Figure 34) of the doors reveal most heat leakage around the door seals. The horizontal seal at the floor and the vertical seal in the middle seem to have the worst thermal bridges in the rear. Could it be that there are metal connections between inside and outside in those locations? On the floor that is the case (Figure 35), but as the same photo shows that seems not the case around the vertical door seal where the two doors meet.

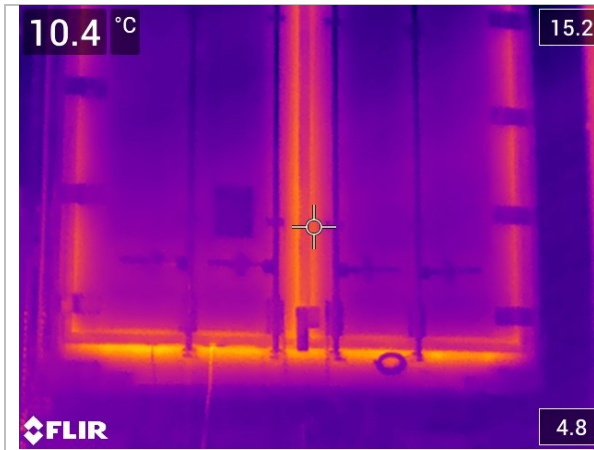


Fig 33 IR photo of lower half of container doors.



Figure 34 IR photo of upper half of container doors.



Figure 35 metal (red) connects inside and outside on the floor. White material is PE (\pm plastic), which should interrupt the metal floor underneath the door, but the door is too thin.

5.2 Supply air flow rate

The supply air flow rate was measured in 13 different test conditions, while the container was empty. Table 11 lists the test conditions and reports the results. In Table 11 column 1 contains just a number assigned to the test condition described in columns 2 till 4. Column 2 is the method of drive: either electric power supply from the 400 V / 50 Hz power grid, or the unit's integrated diesel engine. Column 3 is the evaporate fan speed setting selected in the unit's controller, which has three possible values: either STANDARD, HIGH or MAX. column 4 is the position of wooden panel (Figure 3) in front of the unit's return air grid (Figure 4). The last column lists the measurement results, which are discussed, and compared to manufacturer specs, in section 6.2.

Table 11 *measured air flow rate in a number of test conditions*

No.	method of drive	evap fan speed setting	wooden panel in front of return air grid	measured Φ_{air} [m ³ /h]
1	Diesel	MAX	YES, and drawn into grid	3082
2	Diesel	HIGH	YES, and drawn into grid	2274
3	Diesel	STANDARD	YES, and drawn into grid	1710
4	Electric	STANDARD	YES, and drawn into grid	1804

5	Electric	HIGH	YES, and drawn into grid	2067
6	Electric	MAX	YES, and drawn into grid	2368
7	Electric	MAX	YES, but not drawn into grid	3007
8	Electric	MAX	NO	3852
9	Electric	HIGH	NO	3439
10	Electric	STANDARD	NO	2838
11	Diesel	STANDARD	NO	2875
12	Diesel	HIGH	NO	3946
13	Diesel	MAX	NO	4980

The wooden panel position (column 4) requires some further explanation. At the start of the tests it was installed by Thermo King representatives. Unfortunately, it was then chosen to only install spacers between the wooden panel and the unit's rear at the panel's upper rim and at the panel's two lower corners, but not in the centre of the panel's lower rim. At the start of the supply air flow rate measurements, after completion of all other tests, it was observed that the centre of the wooden panel's lower rim was drawn into the return air grid when the evaporator fans were running. Figure 36 till Figure 38 illustrate this. Just for purpose of illustration a metal bar was put horizontally against the panel's lower rim (Figure 36). At the centre the distance between panel and metal bar was only 4 mm when the unit was off (Figure 37). When the unit was turned on in diesel-drive and evaporator fans speed set to MAX the gap between panel and metal bar in the centre increased till 3 cm (Figure 38).

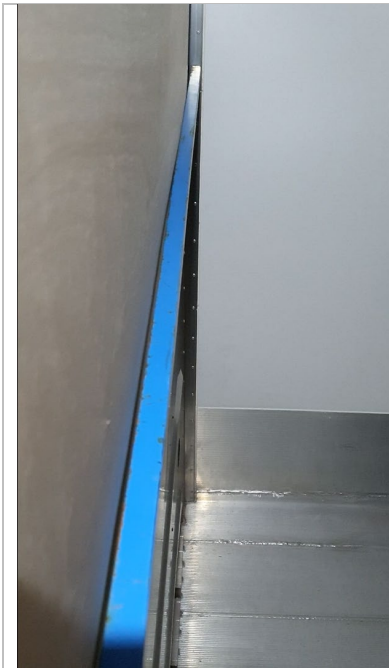


Figure 36 evaporator fan off.

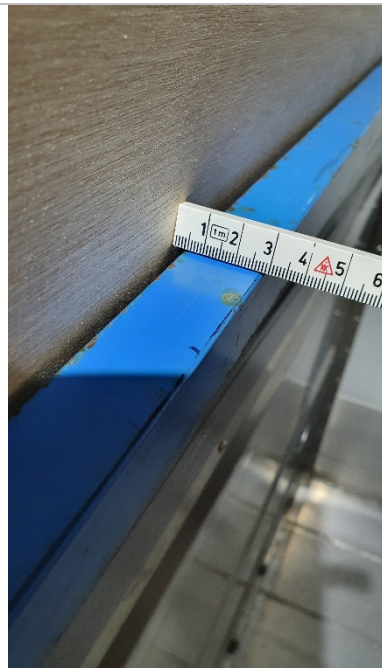


Figure 37 evaporator fan off.



Figure 38 evaporator fan on (diesel, MAX)



Figure 39 the construction used to keep the panel in place during test 7.

5.3 Air velocities and static pressure differences

Air velocities and static pressure differences have only been measured for configuration 1 (reference, see Figure 27) in electric drive. The information received at the time of measurement was that the evaporator fan speed is independent of method of drive. Therefore the measurements were not done in diesel drive. The choice to not measure air velocities and static pressure differences in configuration 2 was a matter of balancing the extra costs/efforts vs. the expectation that it would offer little new insights.

The static pressure differences between the dark green dots and the purple dot in Figure 29 and Figure 30 are listed in Table 12. During the measurements the container doors were closed, the unit ran on 400 V /50 Hz power supply, and the unit setpoint was set equal to the chamber temperature of 20°C. The measurement was repeated three times: for the three possible evaporator fan speeds.

Table 12 *measured pressure difference between location x and door-end: $P_{stat}(x) - P_{stat}(\text{door_end})$ [Pa].*

evaporator fan speed setting:	HIGH	MAX	STANDARD
description of measurement location <input type="checkbox"/>			
Supply air grid	39	49.1	26
Inlet of return air duct	-12.4	-16	-8.2
Pallet 4 bottom left	-10.8	-13	-7

Pallet 8 bottom left	-4.9	-6.8	-2.7
Pallet 12 bottom left	-2.6	-3.1	-1
Pallet 16 bottom left	-1	-1.1	0.1
Pallet 20 bottom left	-0.1	0	0.7
Pallet 24 bottom left	0.8	0.9	1.3

Apart from the supply air grid all measurements are done just above the floor, in the centre of pallet openings. All these 'floor height' measurements are visualized in Figure 40, which is just another way of presenting the information in Table 12.

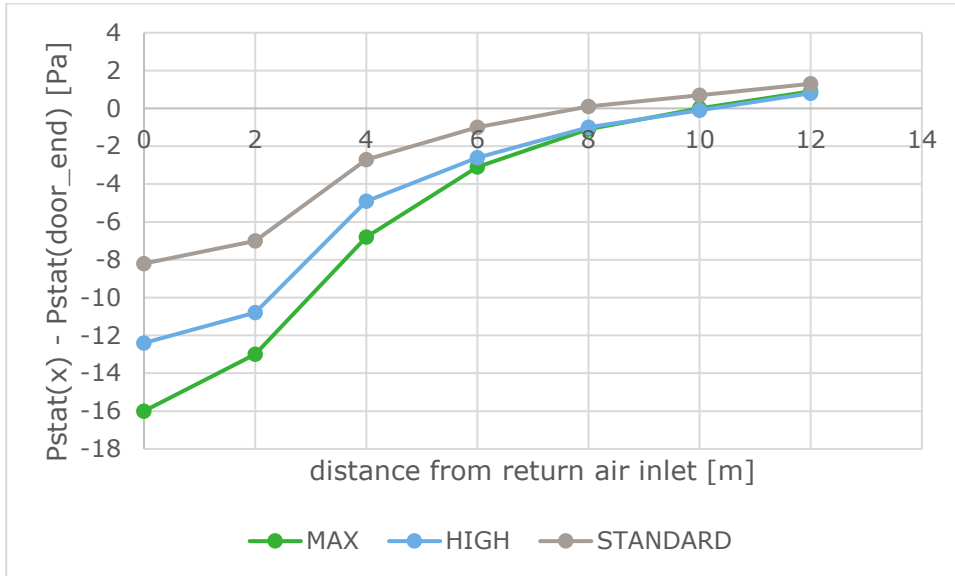


Figure 40 ΔP_{stat} in pallet openings at three different evap. fan speed settings and 400 V / 50 Hz power supply, for configuration 1.

Table 13 and Table 14 present the air velocity measurement data. Figure 41 till Figure 43 graphically present the numbers listed in Table 13 and Table 14.

Table 13 measured air velocities [m/s] above air chute.

distance from unit [m]:	0	1	3	5	7	10	12
evap fan speed MAX	12.16	7.23	5.45	4.32	2.97	1.41	0.02
evap fan speed HIGH	11.06	6.54	4.88	3.81	2.63	1.23	0.02
evap fan speed STANDARD	9.21	5.26	4.03	3.18	2.18	0.98	0.02

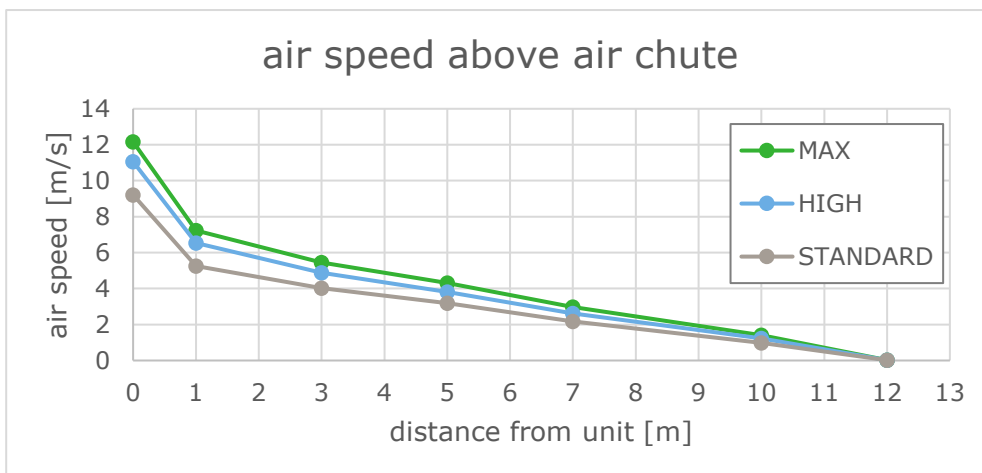


Figure 41 air speed above air chute.

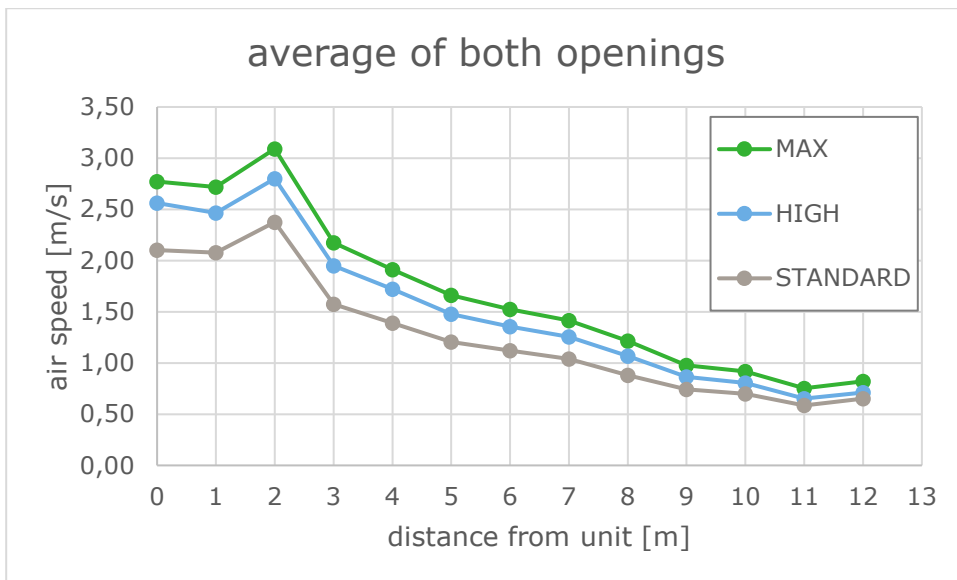


Figure 42 *air velocity in pallet openings, averaged over the left and right opening.*

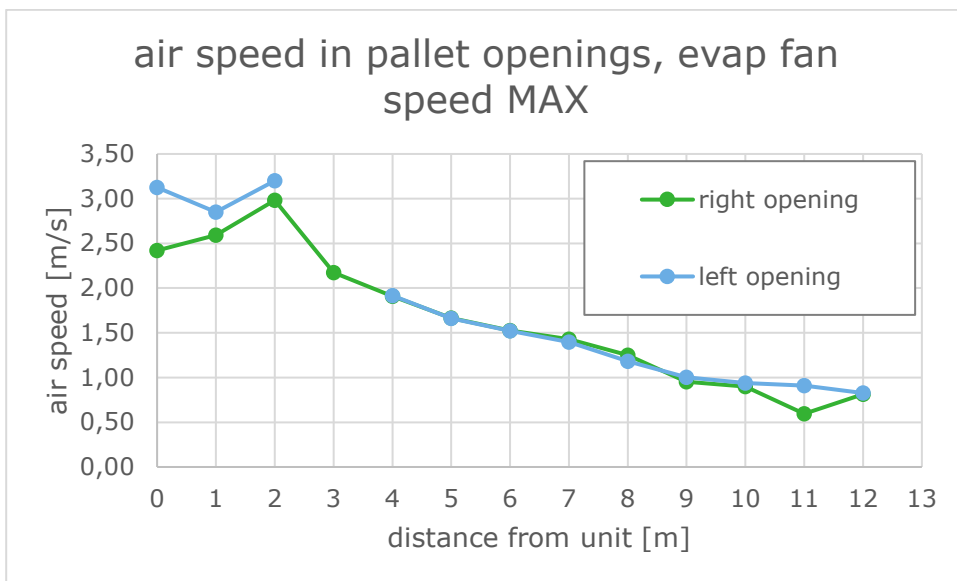


Figure 43 *air speed in both pallet openings at evaporator fan speed MAX.*

Table 14 *measured air velocities [m/s] in center of openings of right row of pallets.*

evap fan speed ↓:	distance from unit [m]:	0	1	2	3	4	5	6	7	8	9	10	11	12
MAX	right opening	2.42	2.59	2.98	2.18	1.91	1.67	1.53	1.43	1.25	0.95	0.90	0.59	0.81
HIGH		2.20	2.35	2.69	1.95	1.70	1.48	1.35	1.27	1.09	0.84	0.78	0.49	0.71
STANDARD		1.77	2.00	2.28	1.57	1.37	1.20	1.11	1.04	0.90	0.74	0.69	0.46	0.65
MAX	left opening	3.12	2.85	3.20	NaN	1.92	1.66	1.52	1.40	1.18	1.00	0.94	0.91	0.83
HIGH		2.93	2.58	2.91	NaN	1.74	1.48	1.37	1.24	1.05	0.88	0.84	0.82	0.71
STANDARD		2.43	2.16	2.47	NaN	1.41	1.21	1.14	1.04	0.86	0.75	0.71	0.71	0.65
MAX	average of both openings	2.77	2.72	3.09	2.18	1.91	1.66	1.52	1.41	1.22	0.98	0.92	0.75	0.82
HIGH		2.56	2.46	2.80	1.95	1.72	1.48	1.36	1.25	1.07	0.86	0.81	0.65	0.71
STANDARD		2.10	2.08	2.38	1.57	1.39	1.21	1.12	1.04	0.88	0.74	0.70	0.59	0.65

5.4 Temperature mapping

Table 15 presents the steady state temperatures measured in the different test conditions. Column 1 till 6 repeat Table 8, and have been explained there. Column 7 lists the duration of the steady state. All temperatures reported in Table 15 are time-averaged readings over the mentioned steady state period. Column 8 (coldest cargo temperature) reports the coldest temperature recorded by any of the sensors taped to the cartons. Column 9 (coldest cargo temperature sensor) indicates which sensor was the coldest. Column 10 (warmest cargo temperature) reports the warmest temperature recorded by any of the sensors taped to the cartons. Column 11 (warmest cargo temperature sensor) indicates which sensor was the warmest. Column 12 (warmest – coldest cargo temp.) reports the highest minus the lowest temperature recorded by the sensors taped to the cartons. Column 13 is the return air temperature, taken as the average of the time-averaged readings of sensors ATP14 and sn269, mounted at the entry of the return air duct (see Figure 31). Column 14 is the supply air temperature, taken as the average of the time-averaged readings of sensors ATP13 and sn284, mounted at the unit’s supply grid (see Figure 31). Column 15 reports the difference $T_{ret}-T_{sup}$. Finally the last column contains the ratio TDF, (warmest – coldest cargo temp.) / $abs(T_{ret}-T_{sup})$, as explained in eqn. 3 on p. 8.

Probably the last two columns are the most interesting: when is $T_{ret} - T_{sup}$ largest (worst)? And what is then the ratio TDF? The results are discussed in further detail in section 6.4.

Just as an illustration the recorded steady state temperatures for a few arbitrarily selected tests are shown in Figure 62 (p. 59) till Figure 64 (p. 60).

Table 15 steady state temperatures observed during tests.

1. T_{set} / T_{amb} [°C]	2. test no.	3. Run mode	4. Method of drive	5. Evap fan speed	6. # pallets	7. steady state duration [d h:mm]	8. coldest cargo temperature [°C]	9. coldest cargo temperature sensor	10. warmest cargo temperature [°C]	11. warmest cargo temperature sensor	12. warmest - coldest cargo temperature [°C]	13. T_{ret} [°C]	14. T_{sup} [°C]	15. $T_{ret} - T_{sup}$ [°C]	16. $(T_{warmest} - T_{coldest}) / \text{abs}(T_{ret} - T_{sup})$
6 / -22°C	6	Continuous	Electric	HIGH	26	11:50	3.2	ATP6	7.8	sn268	4.6	4.2	7.4	-3.2	1.5
6 / -22°C	7	Continuous	Electric	standard	26	22:43	3.1	ATP6	8.3	sn268	5.2	4.0	7.9	-3.8	1.4
6 / -22°C	8	Continuous	Diesel	HIGH	26	12:59	2.9	ATP6	7.2	sn268	4.4	3.7	7.2	-3.5	1.2
22 / -22°C	10	Continuous	Electric	HIGH	26	8:00	17.7	ATP6	25.2	ATP1	7.5	18.6	25.1	-6.5	1.1
22 / -22°C	10B	Continuous	Electric	STANDARD	26	5:00	17.3	ATP6	25.6	sn268	8.3	18.3	25.2	-7.0	1.2
20 / -22°C	11	Continuous	Electric	HIGH	26	8:00	15.5	ATP6	22.6	ATP1	7.1	16.4	22.5	-6.0	1.2
20 / -22°C	12	Continuous	Diesel	HIGH	26	11:11	16.0	ATP6	22.6	ATP1	6.6	17.0	22.6	-5.6	1.2
20 / -22°C	17	Cycle-Sentry	Electric	HIGH	26	4:58	13.2	ATP8	25.3	sn264	12.1	13.8	25.7	-11.9	1.0
20 / -22°C	18	Cycle-Sentry	Diesel	HIGH	26	FAILED									
20 / 20°C	19	Cycle-Sentry	Diesel	HIGH	24	5:20	19.8	ATP15	24.2	ATP6	4.5	21.4	20.6	0.9	5.2
20 / 20°C	20	Cycle-Sentry	Electric	HIGH	24	4:15	20.6	ATP15	21.9	ATP16	1.4	21.1	21.7	-0.7	2.1
20 / 20°C	21	Continuous	Diesel	HIGH	24	4:00	18.7	ATP15	19.1	ATP16	0.4	19.0	18.9	0.1	4.5
20 / 20°C	22	Continuous	Diesel	STANDARD	24	5:22	18.4	ATP3	18.6	ATP6	0.3	18.7	18.6	0.1	2.7
20 / 20°C	23	Cycle-Sentry	Diesel	STANDARD	24	5:59	19.1	ATP16	19.9	ATP3	0.8	19.1	21.5	-2.3	0.3
20 / 40°C	25	Cycle-Sentry	Diesel	HIGH	24	2:49	16.8	ATP3	27.1	ATP7	10.4	21.4	16.3	5.1	2.0
18 / 40°C	26	Continuous	Electric	HIGH	26	12:06	16.0	ATP3	21.7	ATP9	5.6	19.4	16.0	3.4	1.7
20 / 37°C	26A	Continuous	Electric	HIGH	24	4:39	18.1	sn255	22.2	ATP7	4.0	21.0	18.2	2.8	1.5

20 / 40°C	26B	Continuous	Electric	HIGH	24	7:27	18.0	sn255	23.1	ATP7	5.1	21.4	18.1	3.3	1.5
20 / 40°C	27	Continuous	Diesel	HIGH	24	11:00	18.0	ATP1	22.1	ATP7	4.1	21.1	18.0	3.1	1.3
4 / 35°C	31	Continuous	Electric	HIGH	26	2:27	2.1	sn255	11.4	ATP9	9.2	6.4	2.3	4.0	2.3
4 / 40°C	33	Continuous	Diesel	HIGH	26	1:10	2.2	sn255	12.5	ATP9	10.3	6.8	2.3	4.4	2.3
4 / 40°C	33A	Continuous	Diesel	MAX	26	1:00	2.1	ATP1	11.5	ATP9	9.4	6.6	2.0	4.7	2.0
4 / 40°C	33B	Continuous	Diesel	MAX	24	8:35	2.2	ATP1	7.4	ATP7	5.3	6.3	1.9	4.4	1.2
5 / 40°C	33C	Continuous	Diesel	MAX	24	5:40	3.2	ATP1	8.5	ATP7	5.3	7.5	2.8	4.8	1.1
4 / 40°C	33D	Continuous	Diesel	MAX	24	6:00	2.2	ATP1	7.6	ATP7	5.3	6.5	1.8	4.7	1.1
4 / 40°C	39	Cycle-Sentry	Diesel	STANDARD	24	6:15	2.8	ATP3	16.4	sn265	13.5	6.9	3.1	3.8	3.6
4 / 40°C	40	Continuous	Diesel	STANDARD	24	4:00	2.8	ATP3	17.0	ATP8	14.2	7.1	3.2	3.9	3.6

Pull down and pull up tests (Table 9) and power off / door opening / and defrost tests (Table 10) are reported in temperature graphs without further comments (Figure 51 till Figure 61 in annex 1, p. 53). Note that test 30 failed because the unit malfunctioned due to high T_{amb} .

5.5 Fuel consumption and power uptake

Table 16 presents the fuel consumption and power uptake observed during the steady state temperature mappings reported in Table 15, and does some further analysis on those numbers to assess energy efficiency. Column 1 till 7 repeat Table 15, and have been explained there. All numbers reported in columns 8 till 17 in Table 16 are time-averages over the mentioned steady state period. Column 8 lists the heat ingress through the walls, calculated as $K * A * (\text{average measured external temperature} - \text{average measured internal temperature})$. Column 9 reports the unit's electric power uptake [W]. Column 10 contains the unit's diesel consumption (L/h). Power uptake and diesel consumption are heavily affected by condenser air inlet temperature and return air temperature. For sake of completeness these two parameters are reported in columns 12 and 14. Column 13 contains the mean internal temperature, calculated as the average of all temperature sensors placed inside the container. Column 15 lists the effective refrigeration capacity [W] applied during the test period, it equals the heat ingress through the walls (column 8) because that is the only heat source during these tests. Finally column 16 and 17 list the energy *efficiencies*: how much heat is removed from the container per amount of energy used? Column 16 represents the energy efficiency in diesel-drive, expressed as global efficiency R_g [kWh/L], calculated as effective refrigeration capacity divided by the unit's diesel consumption. Column 17 represents the energy efficiency in electric-drive, expressed as Coefficient Of Performance COP [(kW thermal)/(kW electric)], calculated as effective refrigeration capacity divided by the unit's power uptake.

Table 16 fuel consumption and power uptake observed during the steady state temperature mapping tests reported in Table 15.

1. T_{set} / T_{amb} [°C]	2. test no.	3. Run mode	4. Method of drive	5. Evap fan speed	6. # pallets	7. steady state duration [d h:mm]	8. Heat ingress through walls [W]	9. Unit' s electric power uptake [W]	10. Unit' s diesel consumption [L/h]	11. Mean external temp. [°C]	12. Mean condenser inlet temp. [°C]	13. Mean internal temp. [°C]	14. T_{ret} [°C]	15. Effective refrigerating capacity [W]	16. global efficiency Rg [kWh/L]	17. COP [(kW th.)/(kW el.)]
6 / -22°C	6	Continuous	Electric	HIGH	26	11:50	-2051	4217.8	0.0	-21.3	-21.1	6.3	4.2	-2051	N.A.	-0.5
6 / -22°C	7	Continuous	Electric	standard	26	22:43	-2063	4106.6	0.0	-21.3	-21.3	6.4	4.0	-2063	N.A.	-0.5
6 / -22°C	8	Continuous	Diesel	HIGH	26	12:59	-2024	0.0	1.1	-21.3	-19.0	5.8	3.7	-2024	-1.9	N.A.
22 / -22°C	10	Continuous	Electric	HIGH	26	8:00	-3252	5378.7	0.0	-21.2	-21.3	22.4	18.6	-3252	N.A.	-0.6
22 / -22°C	10B	Continuous	Electric	STANDARD	26	5:00	-3250	5303.4	0.0	-21.2	-21.3	22.4	18.3	-3250	N.A.	-0.6
20 / -22°C	11	Continuous	Electric	HIGH	26	8:00	-3061	4941.8	0.0	-21.1	-20.4	20.0	16.4	-3061	N.A.	-0.6
20 / -22°C	12	Continuous	Diesel	HIGH	26	11:11	-3098	0.0	1.3	-21.3	-19.8	20.3	17.0	-3098	-2.4	N.A.
20 / -22°C	17	Cycle-Sentry	Electric	HIGH	26	4:58	-3050	4368.2	0.0	-21.3	-21.0	19.6	13.8	-3050	N.A.	-0.7
20 / -22°C	18	Cycle-Sentry	Diesel	HIGH	26	FAILED										
20 / 20°C	19	Cycle-Sentry	Diesel	HIGH	24	5:20	-191	0.0	0.1	19.3	19.3	21.9	21.4	-191	-2.5	N.A.
20 / 20°C	20	Cycle-Sentry	Electric	HIGH	24	4:15	-138	540.7	0.0	19.4	19.4	21.3	21.1	-138	N.A.	-0.3
20 / 20°C	21	Continuous	Diesel	HIGH	24	4:00	162	0.0	1.1	21.1	21.1	18.9	19.0	162	0.2	N.A.
20 / 20°C	22	Continuous	Diesel	STANDARD	24	5:22	214	0.0	1.1	21.4	21.4	18.6	18.7	214	0.2	N.A.
20 / 20°C	23	Cycle-Sentry	Diesel	STANDARD	24	5:59	88	0.0	0.0	20.7	20.7	19.5	19.1	88	21.8	N.A.
20 / 40°C	25	Cycle-Sentry	Diesel	HIGH	24	2:49	1569	0.0	0.7	42.9	42.9	21.8	21.4	1569	2.3	N.A.
18 / 40°C	26	Continuous	Electric	HIGH	26	12:06	1554	5047.8	0.0	38.8	43.7	18.0	19.4	1554	N.A.	0.3
20 / 37°C	26A	Continuous	Electric	HIGH	24	4:39	1260	4546.6	0.0	36.3	38.5	19.4	21.0	1260	N.A.	0.3

20 / 40°C	26B	Continuous	Electric	HIGH	24	7:27	1446	4785.2	0.0	39.0	42.4	19.6	21.4	1446	N.A.	0.3
20 / 40°C	27	Continuous	Diesel	HIGH	24	11:00	1482	0.0	1.2	39.3	43.5	19.4	21.1	1482	1.2	N.A.
4 / 35°C	31	Continuous	Electric	HIGH	26	2:27	2201	4634.5	0.0	34.2	36.6	4.6	6.4	2201	N.A.	0.5
4 / 40°C	33	Continuous	Diesel	HIGH	26	1:10	2564	0.0	1.4	39.3	44.9	4.9	6.8	2564	1.9	N.A.
4 / 40°C	33A	Continuous	Diesel	MAX	26	1:00	2594	0.0	1.5	39.3	45.1	4.5	6.6	2594	1.7	N.A.
4 / 40°C	33B	Continuous	Diesel	MAX	24	8:35	2635	0.0	1.5	39.3	44.4	4.0	6.3	2635	1.8	N.A.
5 / 40°C	33C	Continuous	Diesel	MAX	24	5:40	2543	0.0	1.5	39.1	44.2	5.0	7.5	2543	1.7	N.A.
4 / 40°C	33D	Continuous	Diesel	MAX	24	6:00	2639	0.0	1.5	39.5	44.4	4.1	6.5	2639	1.8	N.A.
4 / 40°C	39	Cycle-Sentry	Diesel	STANDARD	24	6:15	2384	0.0	0.7	39.9	43.6	7.9	6.9	2384	3.3	N.A.
4 / 40°C	40	Continuous	Diesel	STANDARD	24	4:00	2593	0.0	1.2	43.3	43.3	8.5	7.1	2593	2.1	N.A.

6 Discussion

6.1 K-value + IR photos

The measured K-value of $0.486 \text{ W}\cdot\text{m}^{-2}\cdot\text{°C}^{-1}$ disappoints. In view of measured panel thicknesses a K-value well below the ATP limit of $0.4 \text{ W}\cdot\text{m}^{-2}\cdot\text{°C}^{-1}$ should be feasible. Despite in-depth analysis of design drawings, infrared photos, and lengthy discussions with unit45, at the time of writing of this report it is still unclear why the measured K-value is so high. This certainly deserves further attention from unit45.

6.2 Supply air flow rate

Table 17 lists the manufacturer specs.

Table 17 *supply air flow rate manufacturer spec. (source: Mark Vermeulen, Thermo King, by email on 9-11-2020)*

	Evap fan speed STANDARD	Evap fan speed HIGH	Evap fan speed MAX
Diesel pulldown/up	5000 m ³ /h	5800 m ³ /h	6000 m ³ /h
Diesel at setpoint	3400 m ³ /h	4500 m ³ /h	5500 m ³ /h
Electric pulldown/up	3400 m ³ /h	4000 m ³ /h	4500 m ³ /h
Electric at setpoint	3400 m ³ /h	4000 m ³ /h	4500 m ³ /h

Table 18 is a repetition of the measurements as reported in Table 11, with two columns added: column 6 is the manufacturer's spec for that test condition, taken from Table 17, and column 7 calculates the measured air flow rate (column 5) as percentage of the manufacturer's spec (column 6).

Table 18 *measured air flow rate in a number of test conditions*

No.	method of drive	evap fan speed setting	wooden panel in front of return air grid	measured ϕ_{air} [m ³ /h]	ϕ_{air} [m ³ /h] (manufacturer's spec)	measurement as percentage of spec.
1	diesel	MAX	YES, and drawn into grid	3082	5500	56%
2	diesel	HIGH	YES, and drawn into grid	2274	4500	51%
3	diesel	STANDARD	YES, and drawn into grid	1710	3400	50%

4	electric	STANDARD	YES, and drawn into grid	1804	3400	53%
5	electric	HIGH	YES, and drawn into grid	2067	4000	52%
6	electric	MAX	YES, and drawn into grid	2368	4500	53%
7	electric	MAX	YES, but not drawn into grid	3007	4500	67%
8	electric	MAX	NO	3852	4500	86%
9	electric	HIGH	NO	3439	4000	86%
10	electric	STANDARD	NO	2838	3400	83%
11	diesel	STANDARD	NO	2875	3400	85%
12	diesel	HIGH	NO	3946	4000	99%
13	diesel	MAX	NO	4980	5500	91%

As column 7 illustrates the measurements without wooden panel, i.e. test number 8 till 13, are all within 17% from the manufacturer's spec. In view of the test method's inaccuracy this is interpreted as a confirmation of the correctness of the manufacturer specs. On average the reported air flow rate in test number 8 till 13 is 88% of manufacturer spec.

Test number 1 till 6 all report air flow rates of 50 till 56% of the manufacturer spec. On average the reported air flow rate is 52% of manufacturer spec.

Test number 7 is the only test with the return air duct implemented as intended. Its reported air flow rate is 67% of the manufacturer's spec.

The measured average air flow rates for the three position of the wooden panel in front of the return air grid are 88, 52 and 67% of the manufacturer spec. The measurement procedure is not very accurate. Therefore it is assumed that the difference between manufacturer spec and measured air flow rate without wooden panel are caused by a structural measurement error inherent to the measurement procedure. The differences (88-52)% and (88 - 67)% are caused by the installed wooden panel, correcting these differences for the measurement error assumed at 88% yields the following estimates for the impact of installing the intended return air duct without drawn-in panel (67%) and the improvised return air duct with drawn-in panel (52%):

- Air flow rate with wooden panel drawn in = $100 * (1 - (88-52)/88) = 59\%$ of manufacturer spec.
- Air flow rate with wooden panel in intended position = $100 * (1 - (88-67)/88) = 76\%$ of manufacturer spec.

The intended return air duct reduces the unit's supply air flow rate to 76%. That is a large reduction, and reason to consider a less narrow return air duct. Probably it is wise to (at least) double the depth of the return air duct, i.e. the thickness of the front stop rails, from 5 to 10 cm.

For interpretation of the temperature mapping tests the safest assumption is that during all tests the supply air flow rate has been equal to that of the improvised panel, i.e. 59% of manufacturer spec, although the air flow rate may have been more during the first tests. This assumption ignores the fact that pallet blockers (Figure 3) may also to some (unknown) extent obstruct the air flow from the openings of pallet 1 and 2 into the return air duct.

In conclusion:

1. Without return air duct the measured supply air flow rate is according to manufacturer's specs.
2. The improvised return air duct, with drawn-in wooden panel, reduces the air flow rate till 59% of the manufacturer spec (from 88 to 52 %, taking 88% as reference).
3. The intended return air duct reduces the air flow rate till 76% of the manufacturer spec (from 88 to 67 %, taking 88% as reference). We recommend a better dimensioning of the return air duct, of course without wooden plate improvisation, with a depth of approximately 10 instead of the current 5 cm.
4. For the temperature mapping test the best assumption is that all tests have been executed at the 59% air flow rate.

6.3 Air velocities and static pressure differences

Above the air chute the air speed in longitudinal direction rapidly diminishes towards the door-end (Figure 41): from about 6 m/s at 1 m from the unit till about 1.2 m/s at 10 m. Apparently most air has escaped from the air chute to the sides before it reaches the end of the air chute. Moreover the air velocity at 10 m from the unit-end is only marginally affected by evaporator fan speed. Therefore we recommend to redesign the supply air duct such that it delivers much more air to the door-end.

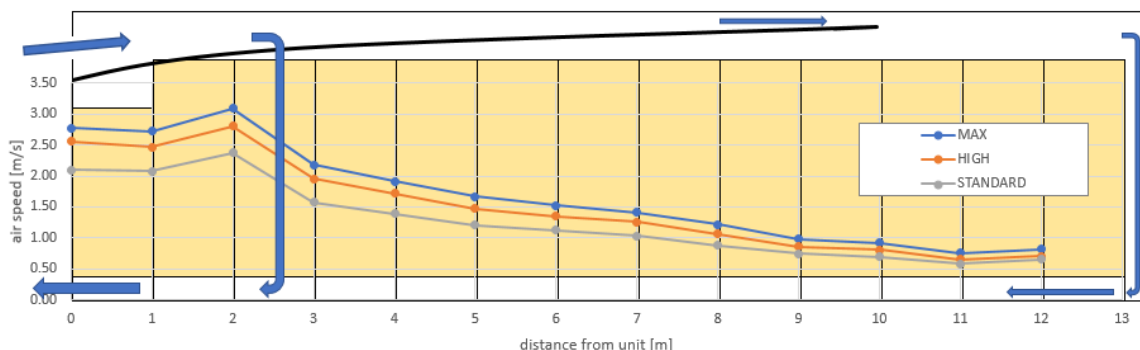


Figure 44 visualisation of air flow distribution: only little air reaches the door-end. The air velocities plotted in this figure are the air velocities measured in the pallet openings, averaged over the left and right opening, as shown in Figure 42.

In the pallet openings the pattern is more or less the same as in the air chute (compare Figure 42 to Figure 41), but is remarkable that the measured velocities in the pallet openings at 0 and 1 m from the unit-end are lower than at 3 m. We are unsure how to explain this. A first option is a strong upward recycle current along the sides of the pallet loads at the unit-end. A second possible explanation is that the air velocity in the pallet opening is measured at half height, while at the unit-end the air velocity in the upper half of the pallet opening is distinctly higher than in the lower half. This might be possible because air is drawn upward into the return air duct and because the pallet stoppers obstruct the air flow on the floor (Figure 45).

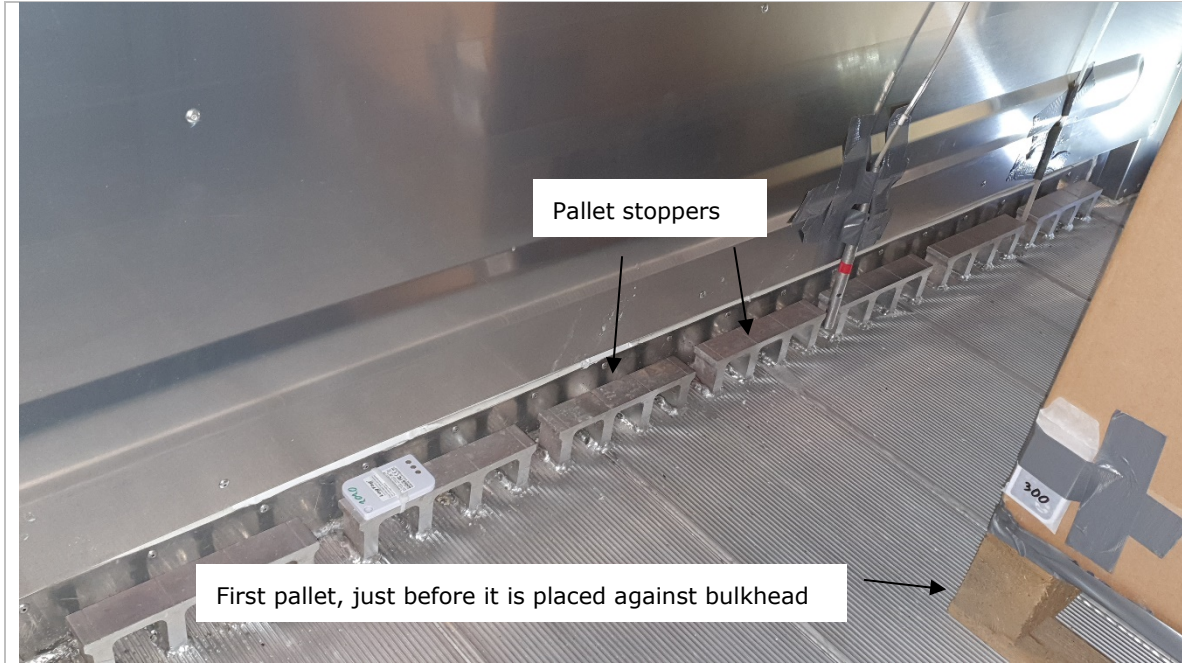


Figure 45 do pallet stoppers obstruct air flow from pallet openings into return air duct?

In the first meters at the unit-end the air velocity in the pallet openings is higher in the left opening (Figure 43), which is more towards the container's centre line. This corresponds with an evaporator inlet which does not at all span the complete container width (Figure 4, Figure 5). To homogenise air velocities across the width at the inlet to the return air duct one should reduce air flow resistance for air entering the duct at the sides or increase air flow resistance for air entering at the centre of the return air duct inlet. This could for example be done by reconsidering the orientation of the front stop rails, supporting the front stop panel, as illustrated in Figure 46 and Figure 47. However the limited amount of air reaching the door-end (Figure 44) is a much bigger concern.



Figure 46 current position/orientation of front stop rails.



Figure 47 potentially improved position/orientation of front stop rails.

6.4 Temperature mapping

6.4.1 General temperature distribution patterns

For a selection of representative cases 3D contour plots are given in annex 2 (p. 61). In heating mode (winter conditions) the coldest temperatures occur at the floor near the door-end (see e.g. Figure 65 on p. 61). In cooling mode (summer conditions) the warmest temperatures occur at the door-end, with a slight tendency of ceiling temperatures a bit warmer than floor temperatures (Figure 71 on p. 64).

6.4.2 Maximal cargo temperature difference ΔT_{cargo}

Column 12 in Table 15 shows that the maximal temperature difference in the container exceeds the maximally acceptable 3°C by far for all the extreme conditions tested. Let us first analyze the heating and cooling mode for the situation which is most relevant to practice: method of drive = diesel and run mode = continuous. In heating mode (test 12, $T_{\text{set}} / T_{\text{amb}} = 20 / -22^{\circ}\text{C}$, 26 pallets) $\Delta T_{\text{cargo}} = 6.6^{\circ}\text{C}$, even though speed is HIGH. In cooling mode (test 33D, $T_{\text{set}} / T_{\text{amb}} = 4 / 40^{\circ}\text{C}$, 24 pallets) a ΔT_{cargo} of 5.3°C was observed, despite MAXimum evaporator fan speed. Reducing the evaporator fan speed to STANDARD in the same test condition even increases ΔT_{cargo} to 14.2°C (test 40). This is much worse than the desired situation of $\Delta T_{\text{cargo}} < 3^{\circ}\text{C}$.

6.4.3 ΔT_{cargo} in heating mode vs. cooling mode.

When is the temperature distribution worse, in heating or cooling mode? In cooling mode. Compare e.g. test 12 (heating mode) to test 33 (cooling mode). The only difference is $T_{\text{set}} / T_{\text{amb}}$: $T_{\text{set}} / T_{\text{amb}} = 20 / -22^{\circ}\text{C}$ in test 12, and $4 / 40^{\circ}\text{C}$ in test 33. Both the ΔT_{cargo} (6.6°C vs. 10.3°C) and the ratio TDF (1.2 vs. 2.3) are distinctly larger in the latter cooling mode test 33. The explanation lies in the effect of top-air delivery in combination with natural convection (warm air is lighter and therefore rises up, cold air is heavier and therefore falls down). It is always a challenge to carry enough air to the door-end, but in systems with top-air delivery the cooling mode is most challenging. Towards the door-end the air velocity reduces, but in heating mode natural convection supports the forced air convection by making the warm supply air stay on top and proceed towards the door-end (Figure 48). In cooling mode when the cold supply air loses velocity on its way towards the door-end natural convection tends to make the cold supply air fall down before reaching the door-end, resulting in a secondary warmer vortex towards the door-end (Figure 49). If the forced air convection is weak due to limited amounts of air reaching the door-end the effect can be surprisingly large. The effect is also a little bit visible in the 3D contour plots in annex 2: in heating mode the isotherms are much more horizontally (e.g. Figure 66 on p. 62), while in cooling mode the isotherms tend to be more vertical towards the door-end (e.g. Figure 70 on p. 64).

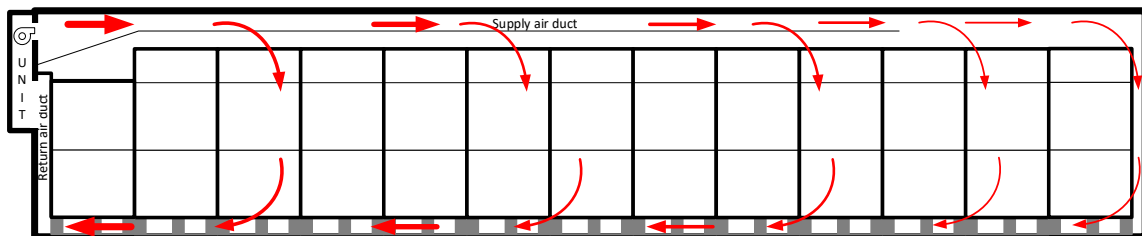


Figure 48 assumed air circulation pattern in heating mode (thicker arrows indicate higher air velocities).

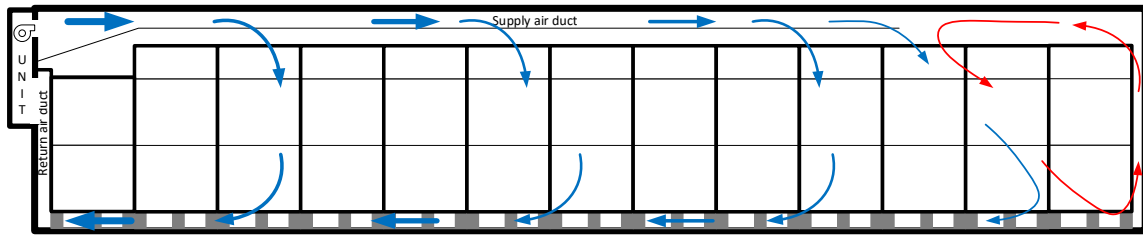


Figure 49 assumed air circulation pattern in cooling mode (thicker arrows indicate higher air velocities).

6.4.4 Effect of evaporator fan speed

Does increasing evaporator fan speed improve temperature homogeneity? Yes, compare e.g. cooling tests 40 and 33D, where evaporator fan speed is the only difference. Evaporator fan speed STANDARD and MAX yield respectively ΔT_{cargo} 14.2 and 5.3°C. Evaporator fan speed MAX instead of STANDARD yields a major improvement in temperature uniformity. Basically the same effect is visible when comparing heating test 6 (HIGH) and 7 (STANDARD). There evaporator fan speeds HIGH and STANDARD yield respectively ΔT_{cargo} 4.6 and 5.2°C.

6.4.5 Air flow distribution

Could a better air flow distribution improve temperature uniformity? Yes, especially in cooling mode. E.g. in test 33 (cooling mode) the ratio TDF, i.e. $\Delta T_{\text{cargo}} / |\Delta T_{\text{unit}}|$, is 2.3, which is significantly higher than the optimal situation of TDF = 1, as explained in section 2. The observed large ratio TDF corresponds with the very low air flow rate at the door-end observed during measurement of air velocities (section 5.3).

6.4.6 Return air temperature control

It looks like the unit uses return air temperature control. E.g. for cooling test 33D ($T_{\text{set}} = 4^{\circ}\text{C}$) the unit's recordings stabilize at $T_{\text{ret}} = 5.4^{\circ}\text{C}$, and $T_{\text{sup}} = 1.8^{\circ}\text{C}$. This probably is return air temperature control, together with top freezing protection (controller parameter 'cont fresh discharge air limit' is set at -2.2°C), resulting in a supply air temperature persistently 2.2°C colder than the set 4°C . That is a recipe for freezing injury in the intercontinental trade, where shippers are used to $T_{\text{sup}} = T_{\text{set}}$. Also in pulldown situations return air temperature control risks freezing injury. Figure 50 illustrates this. The light blue curve in Figure 50 is ATP13, mounted in the supply air grid. During the recovery after defrosting it resides below 0°C for more than 30 minutes, and even drops down to -5°C . At a setpoint of $+4^{\circ}\text{C}$ this is unacceptable for chilled fruit, vegetables, and flower bulbs.

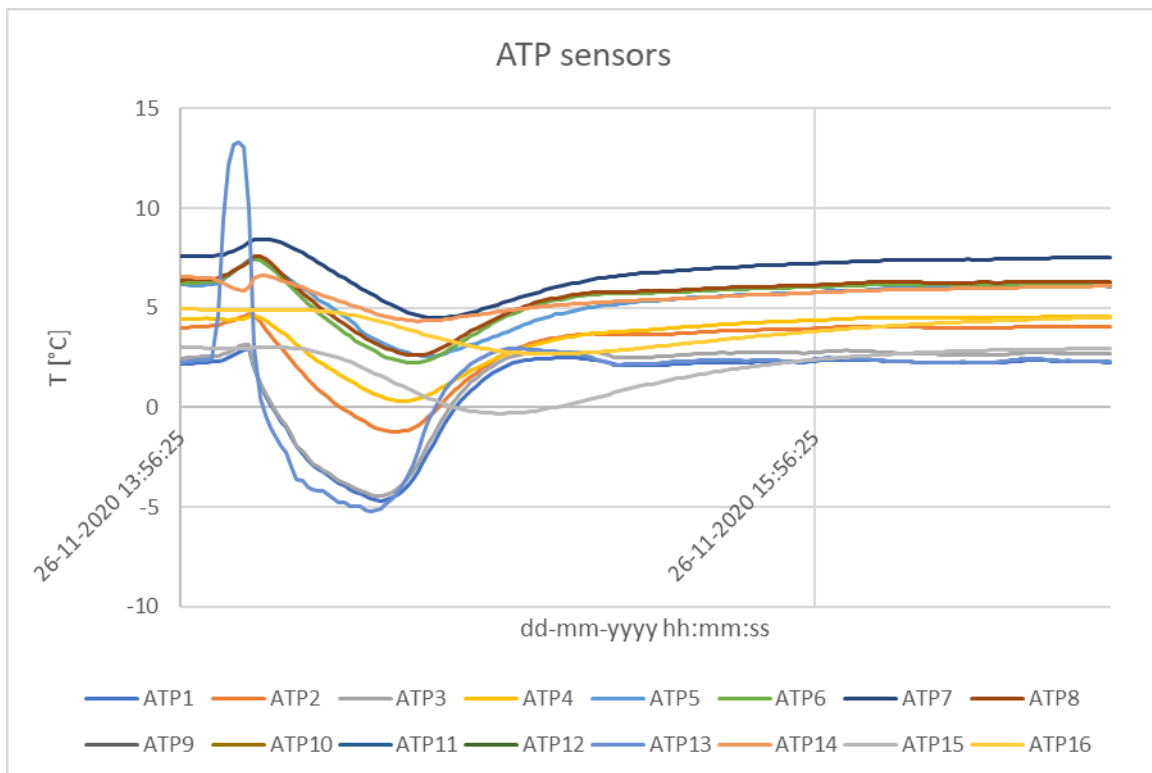


Figure 50 ATP sensor temperature recordings during test 36 (manual defrost + recovery).

Return air temperature control causes cargo temperatures below setpoint. How much below setpoint is uncertain, because it depends on heat load. Therefore return air temperature control is a recipe for freezing injury in chilled range ($T_{set} > -10^{\circ}\text{C}$). It is a good common practice in marine containers in chilled range ($T_{set} > -10^{\circ}\text{C}$) and cooling mode to use supply air temperature control, as opposed to return air temperature control. Supply air temperature control yields tight control over the coldest cargo temperatures, avoids cargo temperatures colder than setpoint, and hence reduces the risk of freezing injury. Also for chilled range cargo in this 45ft rail container supply air temperature control would be preferable in cooling mode.

6.4.7 Effect of 24 or 26 pallets

After test 33A it was decided to proceed to testing with configuration 2 (Figure 28) by removing the two door-end panels. This was done because the ΔT_{cargo} stayed unacceptably high at 9.4°C in test 33A (Figure 71 on p. 64). Just removing the two door-end pallets reduced ΔT_{cargo} to 5.3°C in test 33B (Figure 72 on p. 65). How can these two door-end pallets have such a big impact, while there still is a 15 cm gap between last pallet and door in case of 26 pallets load? Maybe this is just because cargo has been removed from the warmest location. Another factor could be that the door-end air velocities are so low that only a minor decrease of air flow resistances has a significant impact on temperature distribution. This would be an indication that a stronger air flow at the door-end is needed to make the temperature uniformity more robust to minor suboptimalities in cargo stowage. This indication is further supported by the very low air flow rate at the door-end observed during measurement of air velocities (section 5.3).

6.4.8 Effect of run mode

When the temperature difference $T_{set} - T_{amb}$ is large the temperature uniformity may be heavily inflicted by using cycle-sentry mode. Compare e.g. winter tests 11 to 17, where the only difference is run mode: continuous in test 11 and Cycle-Sentry in test 17. The resulting ΔT_{cargo} is respectively 7.1 in test 11 and 12.1°C in test 17. On the other hand the difference between summer test 39 (Cycle-Sentry) and 40 (continuous) is much less pronounced: ΔT_{cargo} is respectively 13.5 in test 39 and 14.5°C in test 40. Another aspect, not reflected in the parameter ΔT_{cargo} is the fierce fluctuation of

temperatures in cycle-sentry mode (see Figure 63 on p. 59). From a temperature point of view cycle-sentry mode is therefore not recommendable for highly temperature sensitive goods like lily bulbs.

6.5 Fuel consumption and power uptake

6.5.1 Global fuel efficiency and COP

During diesel drive the observed global efficiency R_g [kWh/L] ranges between 1 and 2 kWh/L (Table 16, column 16), and diesel consumption in continuous run mode ranges between 1.0 and 1.5 L/h during all tests (Table 16, column 10). Unfortunately we have no access to direct comparison data, but it is our impression that the fuel efficiency is good in comparison to other trailer refrigeration units. During electric drive the best (highest) observed COP in cooling mode is 0.5, which is not very high. It's our impression that also relative to other trailer refrigeration units and to marine container units this is not impressive. Unfortunately for this extreme ambient temperature we have no access to direct comparison data, which makes us hesitate to conclude this firmly.

6.5.2 Cycle-sentry mode

Cycle-sentry mode is a great energy saver compared to continuous run, when heat load is low (compare test 22 and 23). But also in higher heat loads the effect is significant (compare tests 39 and 40, and also see Figure 63 and Figure 64 on page 59). Unfortunately it compromises temperature control too much.

6.5.3 Heating mode efficiency

Normal household electric heating appliances, for example ordinary fan coil heaters, operate with a COP of -1: all electric energy consumed by the device is converted into heat in the space in which it is used. The observed COP in the heating tests (6 till 17) ranges between -0.5 and -0.7. Apparently up to 50% of the consumed electricity is lost in conversion processes before the remainder is dissipated as heat inside the insulated enclosure. The suspicion is that the losses occur in frequency converter(s) and electric motor.

6.5.4 Effect of evaporator fan speed setting

At $T_{set} / T_{amb} = 4 / 40^\circ\text{C}$ and continuous run the measured diesel consumption is 1.2 L/h at evaporator fan speed STANDARD (test 40), 1.4 L/h at evaporator fan speed HIGH (test 33), and 1.5 L/h at evaporator fan speed MAX (test 33B). Apparently reducing evaporator fan speed saves energy in this operating point, which is according to expectation. At $T_{set} / T_{amb} = 20 / 20^\circ\text{C}$ and continuous run the measured diesel consumption is 1.1 L/h both at evaporator fan speed STANDARD (test 22) and at evaporator fan speed HIGH (test 21). We have no explanation for this contradictory and unexpected observation.

6.5.5 Effect of heat load

The fuel consumption seems relatively insensitive to heat load, as long as the run mode is continuous. Test 12, 21 and 33 only differ in T_{set} / T_{amb} , and all run at evaporator fan speed HIGH. Fuel consumption is 1.3 L/h at $T_{set} / T_{amb} = 20 / -22^\circ\text{C}$ (test 12), 1.1 L/h at $T_{set} / T_{amb} = 20 / 20^\circ\text{C}$ (test 21), and 1.4 L/h at $T_{set} / T_{amb} = 4 / 40^\circ\text{C}$ (test 33).

6.5.6 Options to improve energy efficiency

A first setting which is not available and would yet have an added value: run mode HYBRID. Cycle-sentry causes too large temperature oscillations, but has interesting energy savings characteristics, especially in low heat load situations. Therefore we see a window of opportunity for a third run mode: HYBRID. This would then be a run mode in which the continuous run is intermitted in a smart way by sentry-periods during low heat load conditions.

A second setting which is not available and would yet have an added value: evaporator fan speed AUTO. Maximum fan speed gives best temperature uniformity, but usually also the highest energy consumption. This asks for an evaporator fan speed setting AUTO. The idea is that in this setting the evaporator fan speed is continuously adjusted with the purpose to optimized energy consumption, while limiting temperature gradients. Often that would mean something like: MAXIMUM evaporator fan speed in high heat load conditions and (heavily) reduced evaporator fan speed in low heat load conditions.

6.6 Temperature uniformity requirements and feasibility

When it comes to steady state temperature uniformity during lily bulb transport, the overall temperature requirement is that the difference between the warmest and the coldest cargo temperature, ΔT_{cargo} , shall not exceed 3°C when $T_{set} = 0^{\circ}\text{C}$ and $-40 < T_{amb} < 40^{\circ}\text{C}$. What does this imply for the required container insulation (1), the unit's air circulation rate (2) and the air flow distribution (3)?

Since $TDF = \Delta T_{cargo} / \Delta T_{unit}$ (eqn. 3 on p. 8) the temperature requirement

$$\Delta T_{cargo} < 3 \quad [^{\circ}\text{C}] \quad (4)$$

is identical to the overall temperature requirement

$$|T_{ret} - T_{sup}| * TDF < 3 \quad [^{\circ}\text{C}] \quad (5)$$

The above temperature requirement can be split in two separate temperature requirements to be met in steady state when $T_{set} = 0^{\circ}\text{C}$ and $-40 < T_{amb} < 40^{\circ}\text{C}$:

1. $|T_{ret} - T_{sup}| < 2^{\circ}\text{C}$.
2. $TDF < 1.5$.

Note that these two temperature requirements are like communicating vessels: one could be more stringent on $|T_{ret} - T_{sup}|$ and more tolerant on TDF, what counts is that $(T_{ret} - T_{sup}) * TDF$ shall be less than 3°C. The choice for the precise values in these two separate temperature requirements is debatable. Yet there is a good motivation, as will become clear in the remainder of this section and section 6.6.1: these two requirements translate to three equipment requirements which all seem feasible.

The temperature requirement on $|T_{ret} - T_{sup}|$ can be translated to equipment requirements on container insulation and air circulation rate via the overall steady state heat balance over the container's cargo space

$$\frac{\Phi_{circ}}{3600} \times \rho_{air} \times c_{p,air} \times (T_{ret} - T_{sup}) = Q_{trans} + Q_{resp} \quad [\text{W}] \quad (6)$$

With

- Φ_{circ} = air circulation rate [m^3/h]
- $c_{p,air}$ = specific heat of air = 1000 J/kg.°C
- ρ_{air} = air density = 1.3 kg/m³ (@ 0°C)
- T_{ret} = return air temperature [°C]
- T_{sup} = supply air temperature [°C]
- Q_{resp} = cargo's respiratory heat production [W]
- Q_{trans} = heat transfer through the walls [W]

The equation above contains two heat sources Q_{trans} and Q_{resp} . The first heat source, Q_{trans} , can be calculated from

$$Q_{trans} = K \times A \times (T_{amb} - T_{ret}) \quad [\text{W}] \quad (7)$$

With

- K = total heat transfer coefficient [$\text{W} \cdot \text{m}^{-2} \cdot ^{\circ}\text{C}^{-1}$]
- A = mean surface area, which is in this case 153.41 [m^2]
- T_{amb} = ambient air temperature [°C]
- T_{sup} = supply air temperature [°C]

Substitute eqn. 7 in eqn. 6 to get

$$\frac{\Phi_{circ}}{3600} \times \rho_{air} \times c_{p,air} \times (T_{ret} - T_{sup}) = K \times A \times (T_{amb} - T_{ret}) + Q_{resp} \quad [W] \quad (8)$$

The second heat source, the cargo's respiratory heat production Q_{resp} , is the product of specific heat production $q_{resp,spec}$ [W/ton] and the amount of cargo m [ton]:

$$Q_{resp} = q_{resp,spec} \times m \quad [W] \quad (9)$$

For lily bulbs $q_{resp,spec}$ is approximately 10 W/ton. A pallet load of lily bulbs weighs approximately 1 ton. Then a full 45ft load of lily bulbs weighs 26 tons, so $Q_{resp} = 10 \times 26 = 260$ W.

The requirement on $(T_{ret} - T_{sup})$ can be translated to requirements on K and Φ_{circ} . Let us adopt the commonly accepted threshold in view of the ATP treaty for the total heat transfer coefficient. This leads to equipment requirement 1 of 3, specific to the insulation performance of the container box with:

$$K \leq 0.40 \quad [W.m^{-2}.^{\circ}C^{-1}] \quad (10)$$

Then solve eqn. 8 for Φ_{circ} to get

$$\Phi_{circ} = 3600 \times \frac{K \times A \times (T_{amb} - T_{ret}) + Q_{resp}}{\rho_{air} \times c_{p,air} \times (T_{ret} - T_{sup})} \quad [m^3/h] \quad (11)$$

For $K = 0.40$ $W.m^{-2}.^{\circ}C^{-1}$ the requirement $(T_{ret} - T_{sup}) < 2^{\circ}C$ translates to equipment requirement 2 of 3, on the minimum air circulation rate:

$$\Phi_{circ} > 3600 \times \frac{0.4 \times 153.41 \times (40 - 2) + 260}{1.3 \times 1000 \times (2 - 0)}, \text{ i.e. } \Phi_{circ} > 3600 \quad [m^3/h] \quad (12)$$

Finally, equipment requirement 3 of 3 addresses the air flow distribution, which is governed by the design of the supply air duct and the return air duct:

Distribute the air flow such that $TDF < 1.5$, with the ratio TDF defined in eqn. 3 (p. 8).

6.6.1 Feasible of the three equipment requirements

How feasible are these three equipment requirements? Equipment requirement 1 ($K < 0.4$ $W.m^{-2}.^{\circ}C^{-1}$) is met by many types of refrigerated transport equipment in ATP member states and is amply met by standard 40 ft reefers. Despite the large K-value measured for this test container (section 5.1), it should be possible.

Equipment requirement 2 ($\Phi_{circ} > 3600$ m^3/h) should not be too hard. In diesel drive mode at evap fan speed setting MAX the evaporator fans deliver 5500 m^3/h , according to manufacturer spec. The current return air duct reduces that air flow rate to 75% (section 6.2). In section 6.2 we recommend to increase the depth of the return air duct to improve that 75%. On the other hand we recommend to extend the supply air duct (section 6.3). Let us assume that the modified return air duct and the modified supply air duct together still reduce the unit's air circulation rate to 75% of the manufacturer spec. Then in diesel drive mode at evap fan speed setting MAX the evaporator fans will deliver $0.75 \times 5500 = 4125$ m^3/h , according to manufacturer spec. That is well beyond equipment requirement 2 ($\Phi_{circ} > 3600$ m^3/h).

Equipment requirement 3 ($TDF < 1.5$) is a bit less tangible. Section 6.4 discusses a cooling mode test where the observed $TDF = 2.3$. Yet it is believed that just carrying more air to the door-end may help to significantly improve TDF.

Of course also the three equipment requirements are like communicating vessels: one could be more stringent on one requirement, and in exchange more tolerant on the two other requirements.

Note that this section's reasoning does not use safety factors to account for e.g. ageing of insulation, obstructions of air flow, and possible other reasons why in practice the cargo temperature uniformity might be worse than calculated.

6.7 Comparison to other tested containers

How does temperature uniformity achieved in this container compare to other containers? To answer that question see Table 19. Column 1 in Table 19 describes the type of tested container. Column 2 gives the container identification number. Column 3 gives the prime intended application: is it a 40ft marine or a 45ft rail container? Column 4 provides the reference to the report / paper where the tests

are documented. Column 5 and 6 give the container's K- and U-value. Column 7 gives the supply air flow rate calculated from the U-value and the observed ΔT_{unit} (column 15) using eqn. 8. For comparison column 8 mentions the supply air flow rate according to manufacturer's specification. Column 9 describes the container's load during the reported test. In all cases the load existed of pallets stacked with empty cartons. Column 10 presents the unit's temperature setpoint T_{set} and the intended chamber temperature T_{amb} . Column 11 lists the selected run mode. Note that on 40ft marine containers run mode is no choice, it just runs continuous. Column 12 lists the method of drive: diesel in case of 45ft rail, electric (50 Hz / 400 V) in case of 40ft marine because these containers have no diesel engine. Column 13 lists the set evaporator fan speed. Column 14, 15 and 16 present respectively ΔT_{cargo} (eqn. 1), ΔT_{unit} (eqn. 2) and the Temperature Distribution Factor TDF (eqn. 3). The rows in Table 19 lists comparable results in multiple test containers. Row 2 presents test results collected earlier in this project on reference 45ft rail container PVDU380268[0], as reported in Lukasse et al. (2021a). Row 3 presents test results collected earlier in this project on 40ft marine container SUDU806780[1], as reported in Lukasse et al. (2021b). Row 4 adds an extra 40ft marine container test result, as published before in Lukasse & Staal (2018). The last row presents test results documented in this test report (see test 33B in Table 15). For each test container the results for only one test condition are given. Selected are the most favorable results achieved without extra measures to manipulate air flow: no air flow enhancing floor cover, use the air chute if present, select most powerful available method of drive, and select the highest possible evaporator fan speed.

Table 19 steady state temperatures observed during comparable tests in different containers

1. container	2. container no.	3. intended application	4. reference	5. K [W/m ² .°C]	6. U [W/°C]	7. supply air flow rate [m ³ /h] calculated from ΔT_{unit} [°C]	8. supply air flow rate [m ³ /h] (manufacturer spec.)	9. load	10. T_{set} / T_{amb} [°C]	11. Run mode	12. Method of drive	13. Evap fan speed	14. ΔT_{cargo} [°C]	15. ΔT_{unit} [°C]	16. TDF [-]
45ft reference (T1200)	PVDU 380268[0]	45ft rail	Lukasse et al. (2021a)	0.474	71	1654	2400	with air chute and 24 (100 x 120 cm) pallets + 2 (80 x 120 cm) pallets	4 / 40	Continuou s	Diesel	auto (= low)	7.7	4.3	1.8
40ft (Magnum Plus)	SUDU 806780[1]	40ft marine	Lukasse et al. (2021b)	0.383	51	4224	4000	21 (100 x 120 cm) pallets, two blocks-of-four at unit-end	0 / 38	Continuou s	Electric (50 Hz / 400 V)	High	5.1	1.2	4.1
40ft (undisclosed)	undisclosed, half year old	40ft marine	Lukasse & Staal (2018)	unknown	unkno wn	unknown	unknown	20 (100 x 120 cm) pallets	5 / 45	Continuou s	Electric (50 Hz / 400 V)	High	2.8	2.1	1.3
45ft new (Advancer A-500)	PVDU 385011[6]	45ft rail	this report	0.486	75	1689	5500	with air chute and 24 (100 x 120 cm) pallets	4 / 40	Continuou s	Diesel	MAX	5.3	4.4	1.2

The observed ΔT_{cargo} in the new 45ft rail container is 5.3°C (Table 19), while in the reference 45ft rail container $\Delta T_{cargo} = 7.7^\circ\text{C}$. Hence the new 45ft rail container has a better temperature uniformity, but it disappoints in view of the huge increase in supply air flow rate according to manufacturer’s specification. Our own flow rate calculation (column 7) indicates that flow rate in the new 45ft rail container is \pm equal to flow rate in the test container. Why is the flow rate so disappointing? The narrow and improvised return air duct chokes the unit (section 6.2). Also the new 45ft rail container’s K-value disappoints (see section 6.1). It should not be too difficult to largely improve both the K-value and the supply air flow rate. In that way it should be possible to reduce ΔT_{unit} from the current 4.4°C (Table 19) to less than 2°C. With the nice TDF of only 1.2 (Table 19) this would enable the carriage of 24 pallets of lily bulbs in the new 45ft rail container. With an improved air chute design, i.e. improved TDF, even the carriage of 26 pallets may be feasible without violating the requirement $\Delta T_{cargo} < 3^\circ\text{C}$.

Upfront the perception was that the 45ft rail containers would have distinctly worse temperature uniformity than 40ft marine containers. This is because the 40ft marine containers are known to have a lower K-value, a strong supply air flow rate, and a good air flow distribution system (T-bar floor). The observations $\Delta T_{\text{cargo}} = 5.1^{\circ}\text{C}$ and TDF = 4.1 in the 40ft (Magnum Plus) container are surprisingly large, and this makes those test result only marginally better than the ΔT_{cargo} observed in the new 45ft rail container. Therefore another, published, test result is added to Table 19: 40ft (undisclosed) with a load of 20 pallets. In that container test the observed ΔT_{cargo} is 2.8°C and TDF = 1.3. We believe these numbers are more typical of 40ft marine containers. What explains the poor results in the 40ft (Magnum Plus) tests? Most likely pallet number 21 is the main cause.

Is it reasonable to expect that temperature uniformity in improved versions of the new 45ft rail container can be comparable to temperature uniformity in 40ft marine containers? Yes, just improve the return air duct and the K-value. With an improved air chute design, i.e. improved TDF, even the ΔT_{cargo} in a load of 26 pallets may be comparable to the ΔT_{cargo} currently observed in 40ft (undisclosed) marine container with 20 pallets.

In summary. When loaded with 24 pallets and using optimal settings $\Delta T_{\text{cargo}} = 5.3^{\circ}\text{C}$. This is 2.4°C smaller than in the reference 45ft rail container and comparable to ΔT_{cargo} in a 40ft marine container loaded with 21 pallets. After some, probably not too difficult, improvements in return air duct, K-value, and air chute expect $\Delta T_{\text{cargo}} < 3^{\circ}\text{C}$, possibly even in a load of 26 pallets. This would be comparable to ΔT_{cargo} in a 40ft marine container loaded with 20 pallets and meet the requirement for lily bulb transport.

7 Conclusions

1. The measured K-value of $0.486 \text{ W}\cdot\text{m}^{-2}\cdot\text{°C}^{-1}$ disappoints. In view of measured panel thicknesses a K-value well below the ATP limit of $0.4 \text{ W}\cdot\text{m}^{-2}\cdot\text{°C}^{-1}$ should be feasible.
2. Without return air duct the measured supply air flow rate is according to manufacturer's specs.
3. The intended return air duct reduces the air flow rate till 76% of the manufacturer spec (from 88 to 67 %, taking 88% as reference).
4. Too little supply air reaches the door-end, illustrated by a ratio TDF (warmest – coldest cargo temp.) / $\text{abs}(T_{\text{ret}} - T_{\text{sup}})$ of 2.3 in some test conditions.
5. The temperature differences inside the container are too large, especially in cooling mode. In cooling mode at $T_{\text{set}} / T_{\text{amb}} = 4 / 40\text{°C}$, method of drive = diesel, and run mode = continuous, even when the load is reduced to 24 pallets and the evaporator fan speed is set to MAXimum (warmest – coldest cargo temp.) is still 5.3°C . This is worse than the desired situation of (warmest – coldest cargo temp.) $< 3\text{°C}$.
6. Cycle-sentry mode is a great energy saver, especially when heat load is low, but the adverse effect on temperatures is too large to use it during the carriage of highly temperature sensitive goods like lily bulbs.
7. In diesel drive and continuous run mode the observed diesel consumption ranges from 1.0 to 1.5 L/h for the different test conditions. Though we lack precise comparison data, it is our impression that this is a good fuel efficiency in comparison to other trailer refrigeration units.
8. In electric drive and continuous run mode the observed COP in cooling mode is 0.5. The observed COP in the heating tests ranges between -0.5 and -0.7. These numbers do not impress, compared to normal household electric heating appliances operating with a COP of -1. Though we lack precise comparison data, it is our impression that also relative to other trailer refrigeration units and to marine container units this is relatively poor.
9. Increasing evaporator fan speed improves temperature homogeneity, (often) at the cost of increased fuel consumption.
10. A complete dataset of temperatures, air velocities, and static pressure differences has been collected. These data should suffice for accurate CFD model calibration.
11. When loaded with 24 pallets and using optimal settings $\Delta T_{\text{cargo}} = 5.3\text{°C}$. This is 2.4°C smaller than in the reference 45ft rail container and comparable to ΔT_{cargo} in a 40ft marine container loaded with 21 pallets. After some, probably not too difficult, improvements in return air duct, K-value, and air chute expect $\Delta T_{\text{cargo}} < 3\text{°C}$, possibly even in a load of 26 pallets. This would be comparable to ΔT_{cargo} in a 40ft marine container loaded with 21 pallets, and meet the requirement for lily bulb transport.

8 Recommendations

Modifications are needed to meet the temperature uniformity requirement that the difference between the warmest and the coldest cargo temperature shall never be more than 3°C. The measured K-value of 0.486 W.m⁻².°C⁻¹ disappoints, the air chute guides a too little share of the supply air to the door-end, and the return air duct squeezes the air circulation rate too much. It should not be too hard to reduce K to less than 0.40 W.m⁻².°C⁻¹, to redesign the air chute such that a larger share of the supply air reaches the door-end, and to create a less narrow return air duct. These three measures may suffice to meet the temperature uniformity requirement. Below follows a concrete list of recommendations to the relevant stakeholders.

Recommendations to Thermo King:

1. Supply air temperature control in chilled mode. It is a good common practice in marine containers in chilled range ($T_{\text{set}} > -10^{\circ}\text{C}$) and cooling mode to use supply air temperature control, as opposed to return air temperature control. This avoids freezing injury and shippers are used to it. In heating mode in chilled range some manufacturers automatically switch to return air temperature control, again to avoid freezing injury. Copy that practice for trailer units, at least when these are mounted on 45ft reefers destined for longer trips. The risk of freezing injury is simply too big when applying return air temperature control to perishable products in chilled range.
2. Evaporator fan speeds control: adjust to heat load.
3. Need to heat? First increase evaporator fan speed, then apply hot gas heating. In terms of energy consumption it may not make much difference, but higher evaporator fan speed at least yields more uniform cargo temperatures.
4. Remember the smaller(?) practical issues (e.g. socket position and protection) pointed out in ppt in earlier meetings.
5. Consider run mode HYBRID and evaporator fan speed setting AUTO, as described in section 6.5.

Recommendations to unit45:

6. Pallet stoppers (Figure 3 on p. 10) are pallet breakers. Moreover they obstruct to some extent the air flow from the openings of pallet 1 and 2 into the return air duct (Figure 45 on p. 39). Remove the pallet stoppers and instead extend the three front stop rails, supporting the front stop panel, all the way to the floor.
7. Place the four drain holes in the corners of the container floor.
8. Reduce the insulation value of the container to below 0.4 W.m².°C⁻¹, or even further.
9. Properly complete the return air duct, such that the unit can only draw return air from the floor. A return air duct like Figure 5 on p. 11 is unacceptable and ineffective.
10. Significantly increase the depth of the return air duct, i.e. the thickness of the front stop rails, e.g. (at least) double the depth from 5 to 10 cm.
11. Reconsider the length and orientation of the front stop rails (Figure 47)
12. Stop the use of thin doors. The position of the PE strip in the door frame is tailored to the use of thick(er) doors, and it is illogical to have the least insulation in the area where air flow is worst.
13. Increase the door insulation thickness to at least 70 mm. Consider the use of (outward) corrugations on the door's inner cladding to guarantee some space for air circulation between last pallet and door.

Recommendations to Essers(?):

14. Redesign the supply air duct such that it delivers much more air to the door-end.
15. Don't try to use cycle-sentry mode when carrying temperature sensitive goods like lily bulbs.

Literature

- ATP (2020). Agreement on the international carriage of perishable foodstuffs and the special equipment to be used for such carriage. Available from <https://www.unece.org/trans/main/wp11/atp.html>.
- EN16440-1 (2015). Testing methodologies of refrigerating devices for insulated means of transport – Part 1: mechanical cooling device with forced air circulation evaporator with or without heating device.
- Lukasse L.J.S.; Staal M.G. (2018). Optimizing air flow distribution in maritime refrigerated containers. *Acta Hortic. 1194. ISHS 2018. DOI 10.17660/ActaHortic.2018.1194.195. Proc. VIII International Postharvest Symposium: Enhancing Supply Chain and Consumer Benefits – Ethical and Technological Issues. Eds.: F. Artés-Hernández et al.*
- Lukasse L.J.S.; Staal M.G.; Wissink E.B. (2019). An air flow enhancing floor cover to improve temperature uniformity in maritime refrigerated containers. *Proc. of 25th int.'l conf. of refrigeration*, Montreal, Canada, paper ID 54. DOI: 10.18462/iir.icr.2019.0054
- Lukasse L. J. S., Staal M. G., Wildschut J. (2021a). Temperature uniformity, air flow and air pressure in a 45ft reefer container - Climate chamber tests on 45ft intermodal refrigerated container PVDU380268[0]. Wageningen UR Food & Biobased Research report no. 2211.
- Lukasse L. J. S., Staal M. G., Paillart M.J.M. Wildschut J. (2021b). Temperature uniformity and air flow distribution in a 40ft reefer container - Climate chamber tests on 40ft maritime refrigerated container SUDU806780[1]. Wageningen UR Food & Biobased Research report no. 2178.

Acknowledgements

We thank all partners for their financial support and their kind cooperation in facilitating this large test series. Anthos provided the dummy load. Thermo King taught us how to operate the unit, enabled us to collect the unit data, and was always quick in assistance whenever needed. Essers kindly made its container available for many weeks of testing and participated in defining the test plan. Unit45 participated in defining the test plan and assisted in analysing the measured K-value.

Annex 1 Temperature graphs

Figure 51 and Figure 52 show all recorded temperatures during the pull down and pull up tests (Table 9 on p. 23). The legends correspond with the naming of temperature sensors in Figure 29 and Figure 31. Basically the recorded temperatures are clustered in two bundles: a small bundle of three recordings outside the container, and all others inside the container. The internal recordings with the fastest response are the ones most directly exposed to the refrigeration unit's supply air flow.

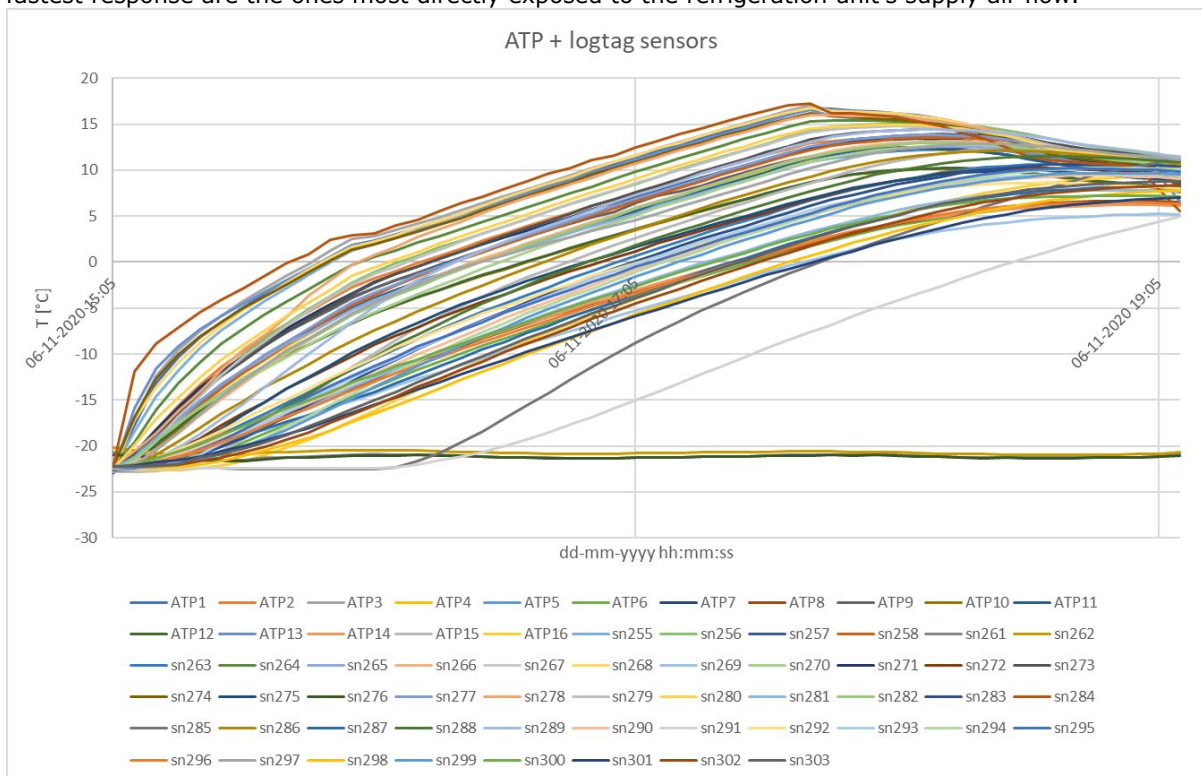


Figure 51 test 5 all temperatures.

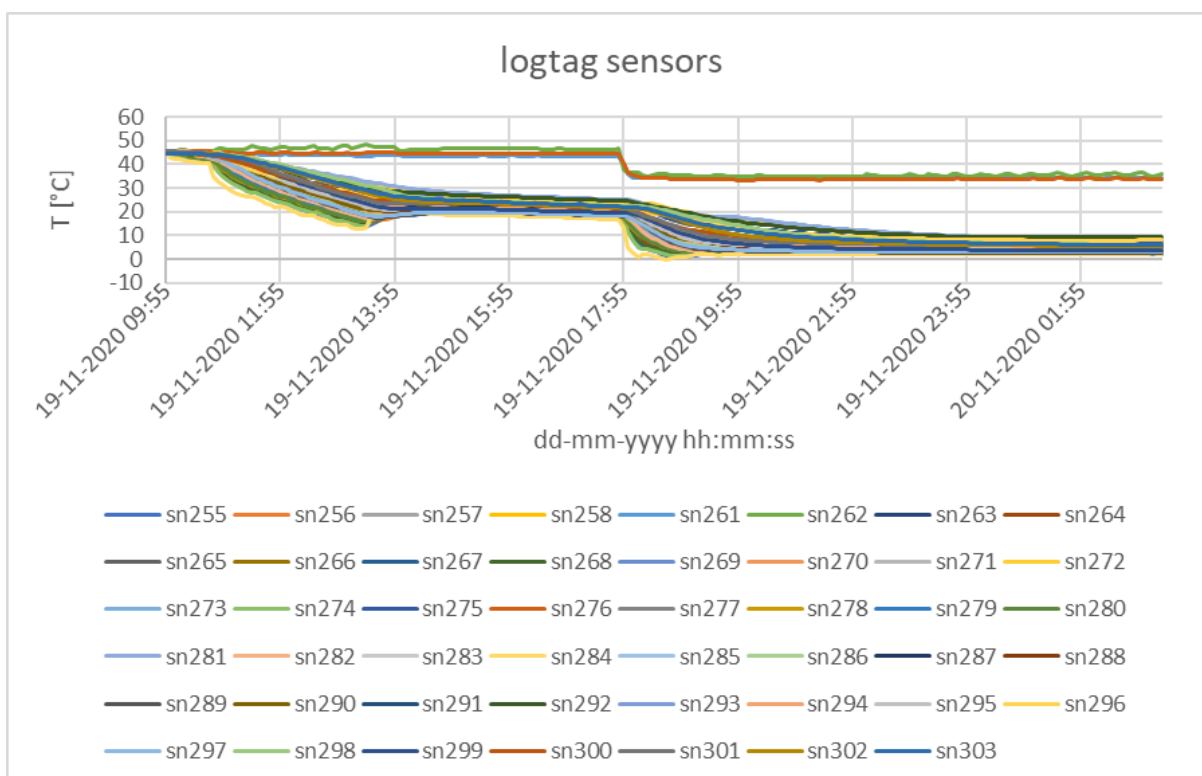


Figure 52 test 30 LogTag temperatures.

Figure 53 till Figure 61 show all recorded temperatures during the tests on power off/ door opening / defrost (Table 10 on p. 24). The legends correspond with the naming of temperature sensors in Figure 29 and Figure 31. Basically the recorded temperatures are clustered in two bundles: a small bundle of three recordings outside the container, and all others inside the container.

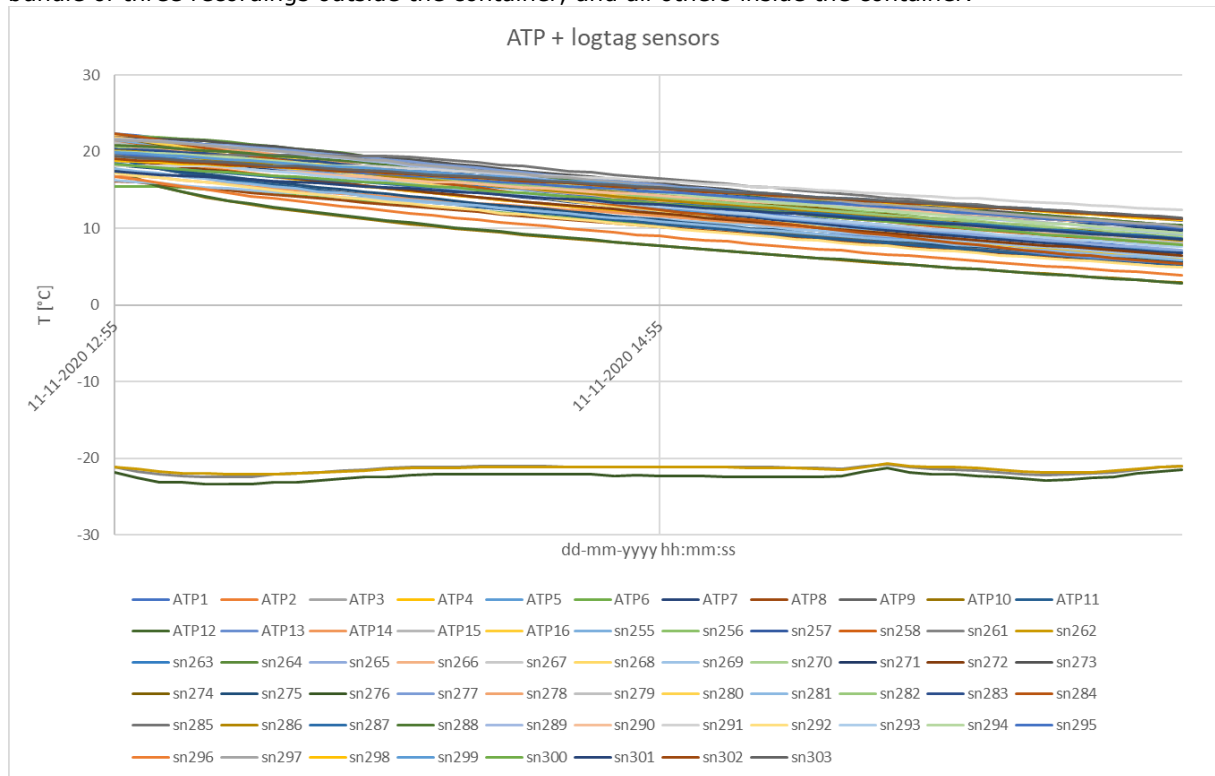


Figure 53 test 13 all temperatures

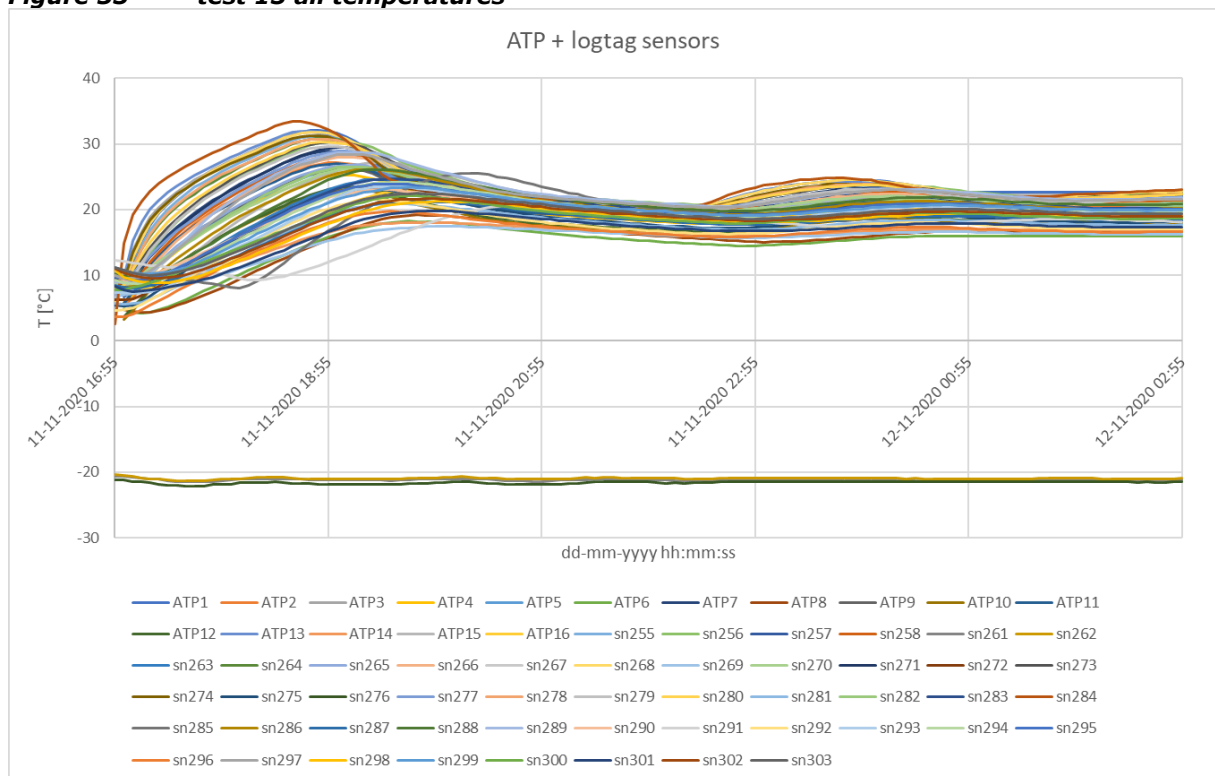


Figure 54 test 14 all temperatures.

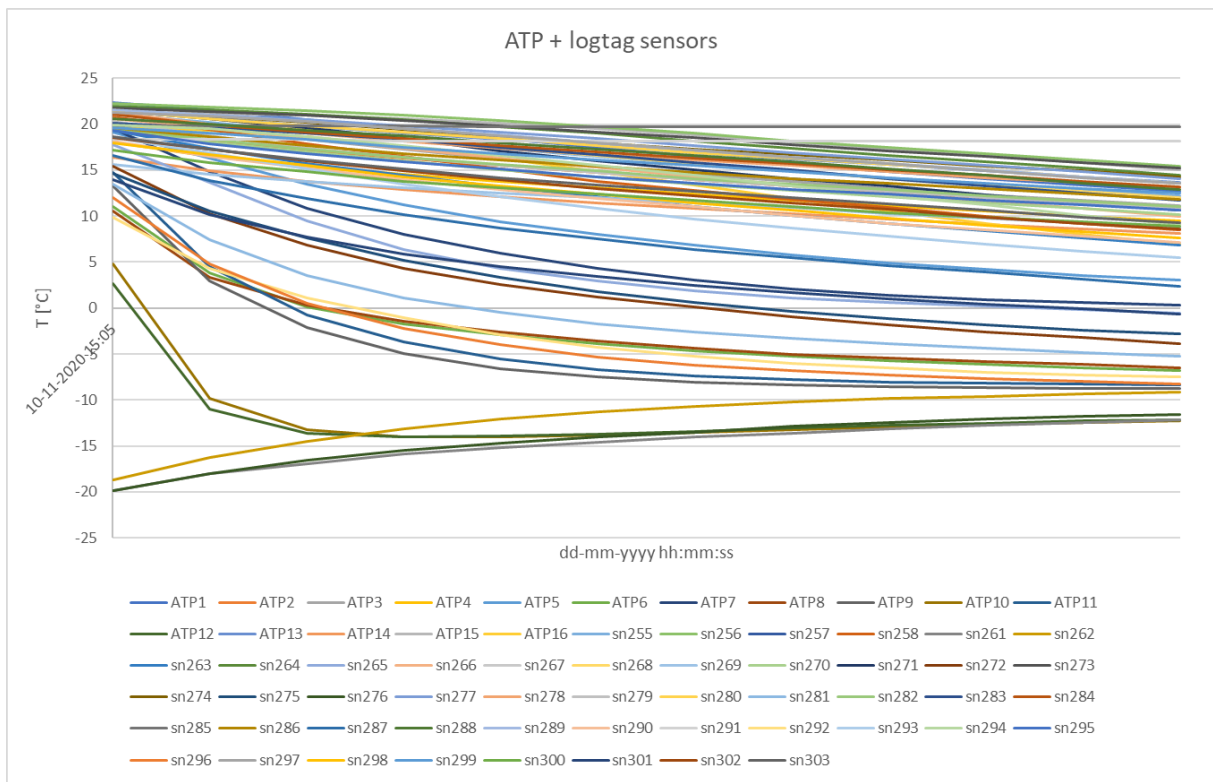


Figure 55 test 15 all temperatures

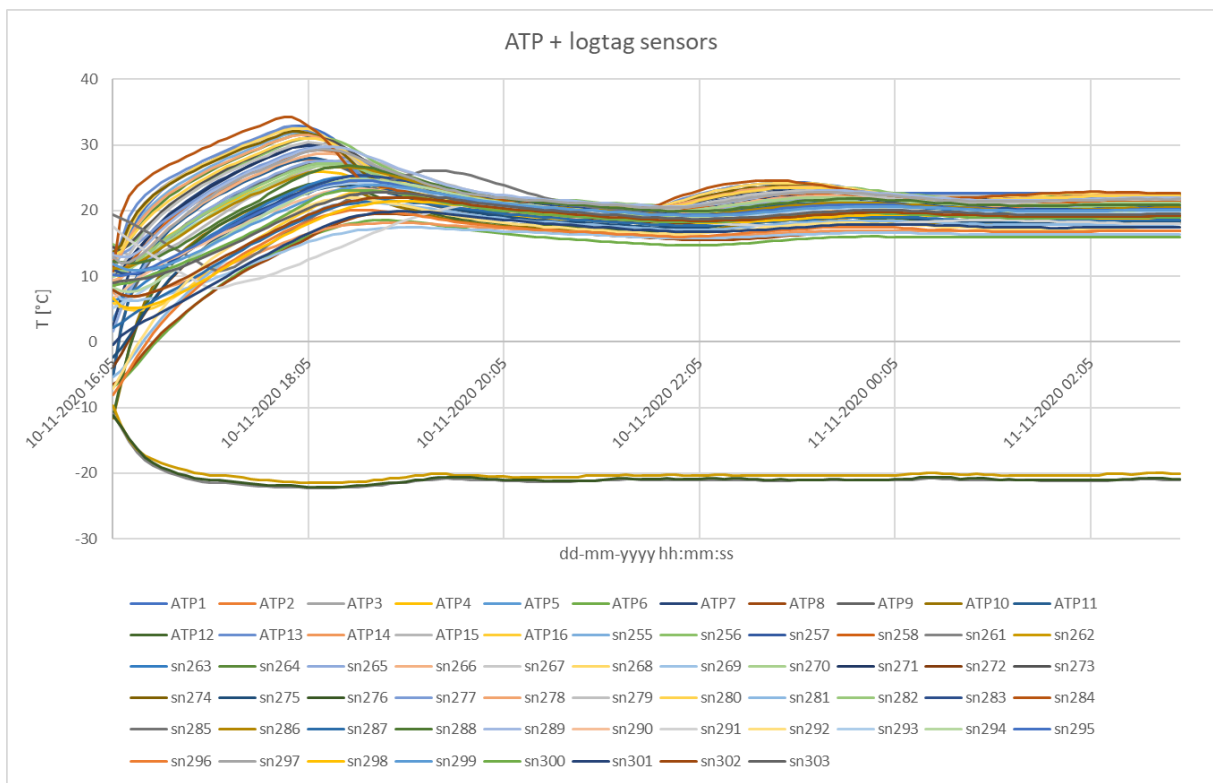


Figure 56 test 16 all temperatures.

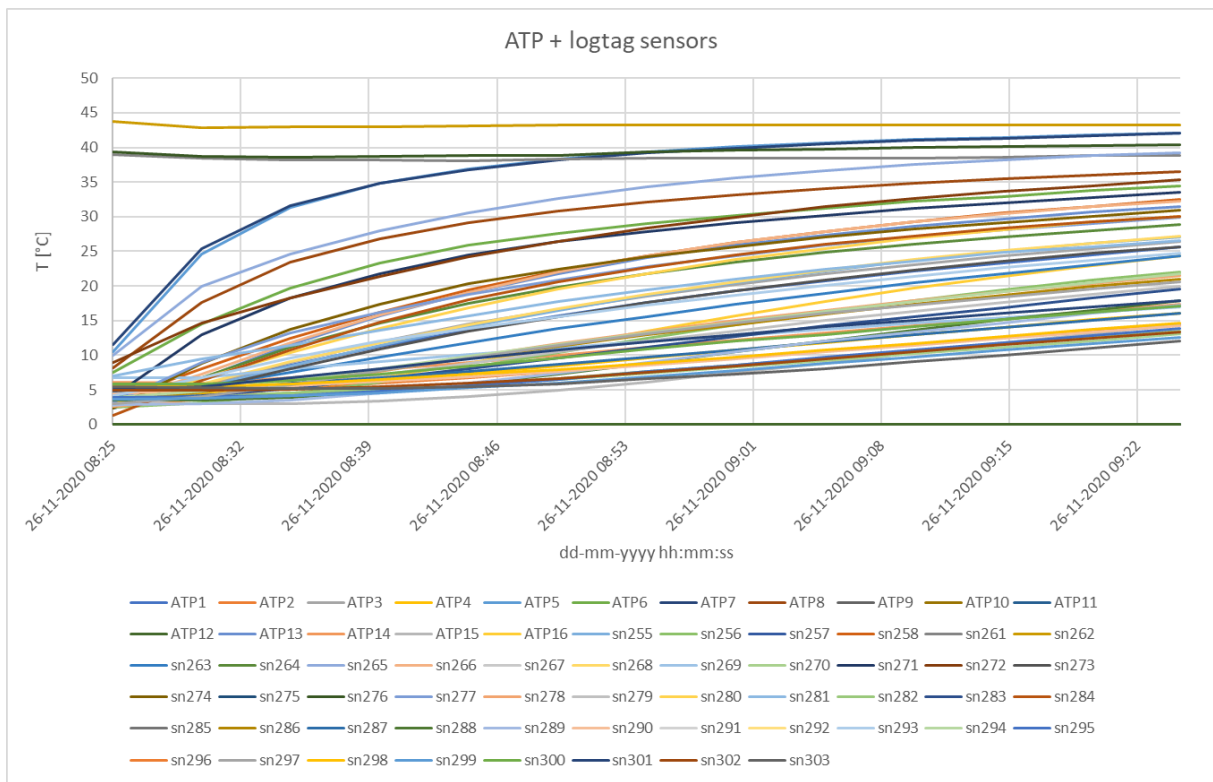


Figure 57 test 34 all temperature data.

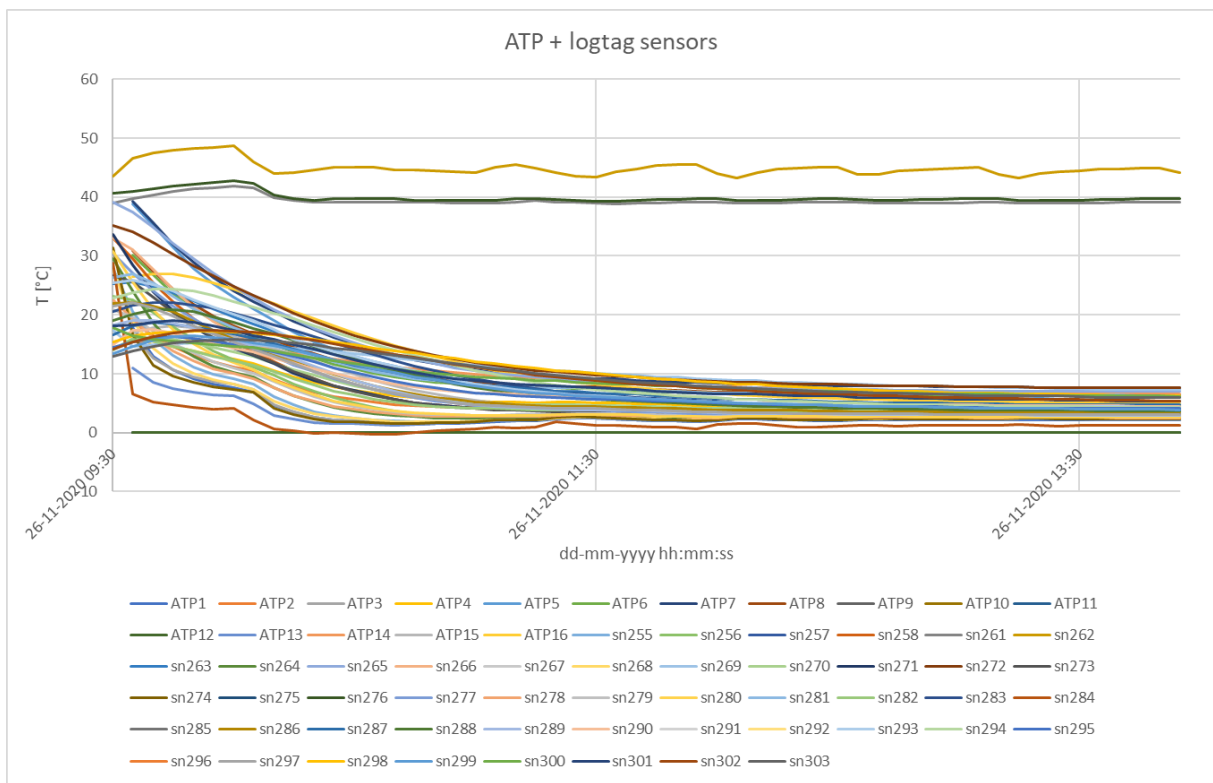


Figure 58 test 35 all temperature data.

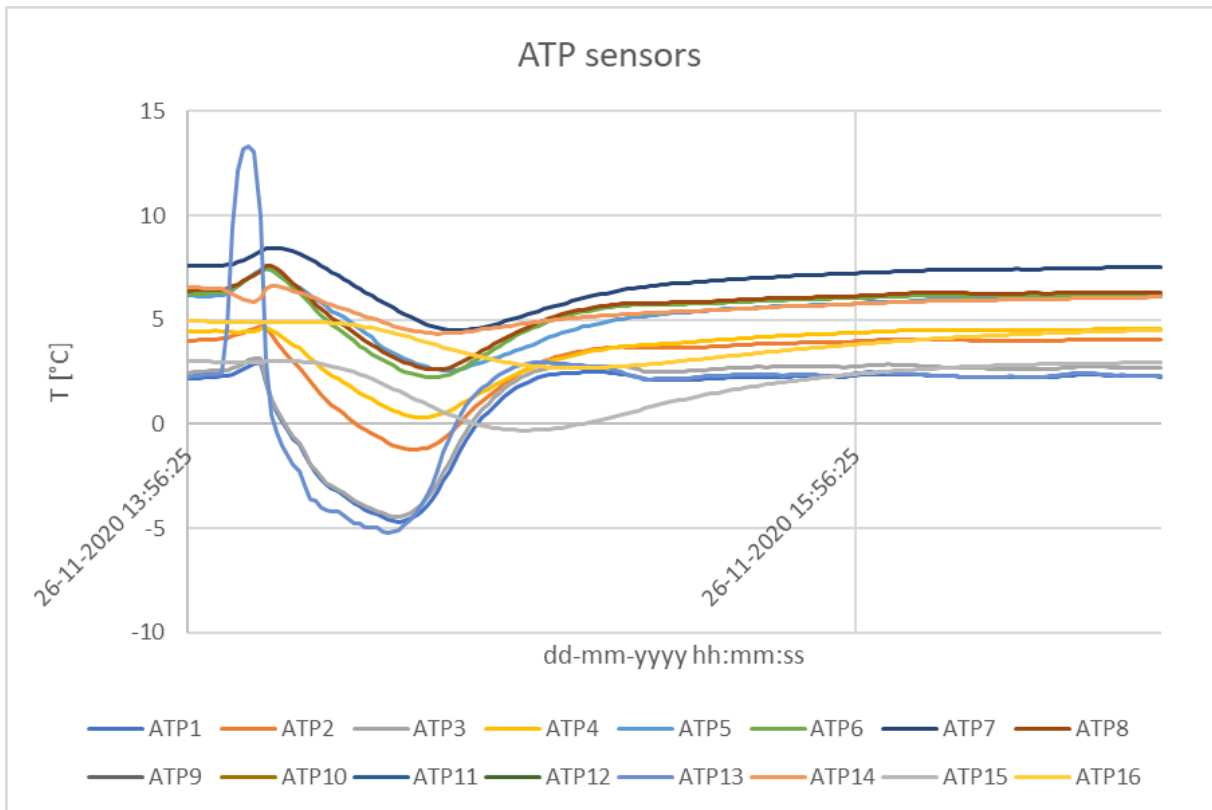


Figure 59 test 36 ATP sensor temperature data.

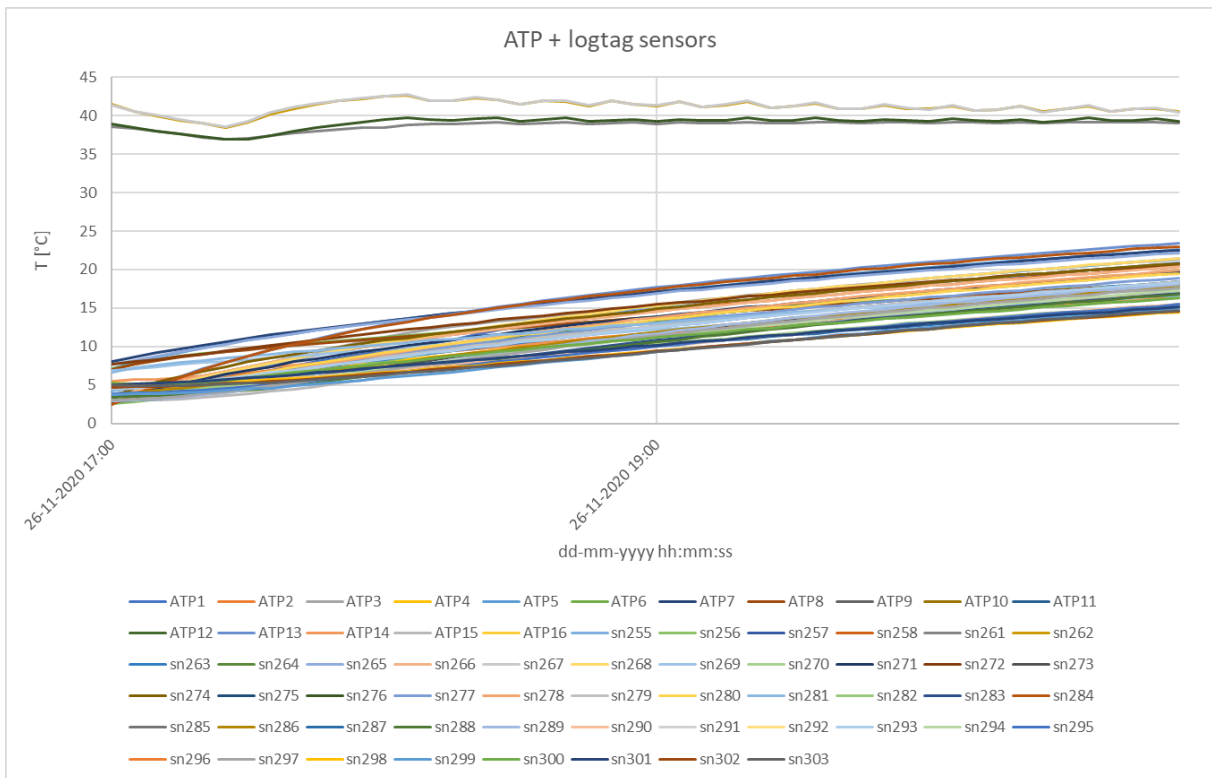


Figure 60 test 37 temperature data.

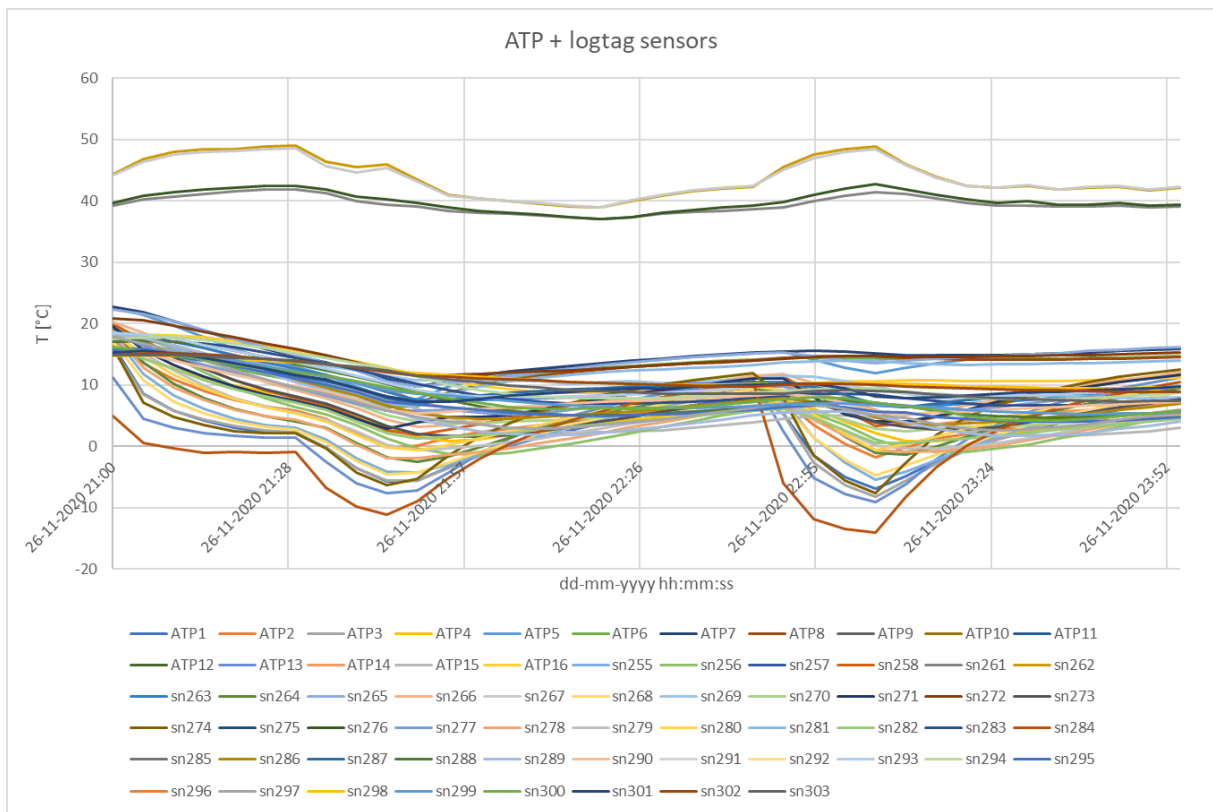


Figure 61 test 38 all temperature data.

Figure 62 till Figure 64 show the recorded temperatures during an arbitrary selection of steady state tests (Table 8 on p. 22). The legends correspond with the naming of temperature sensors in Figure 29 and Figure 31. Basically the recorded temperatures are clustered in two bundles: a small bundle of three recordings outside the container, and all others inside the container.

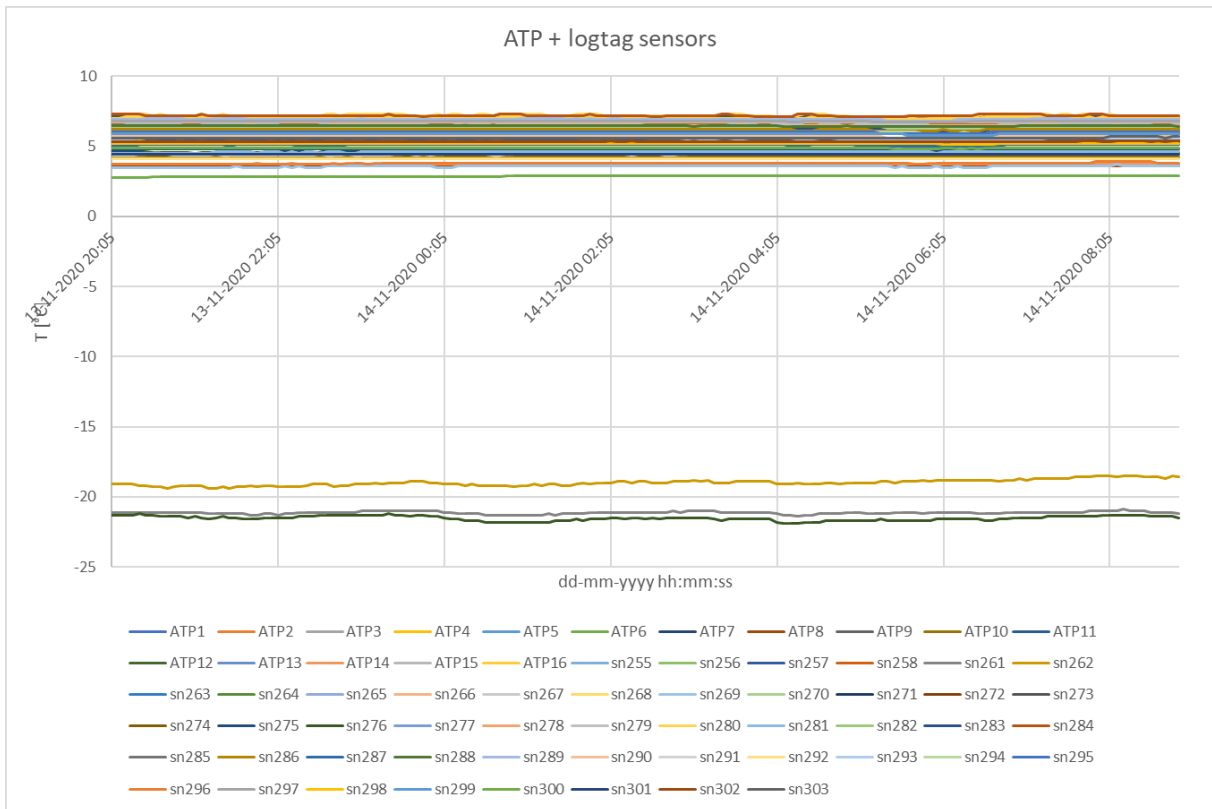


Figure 62 recorded steady state temperatures for test 8.

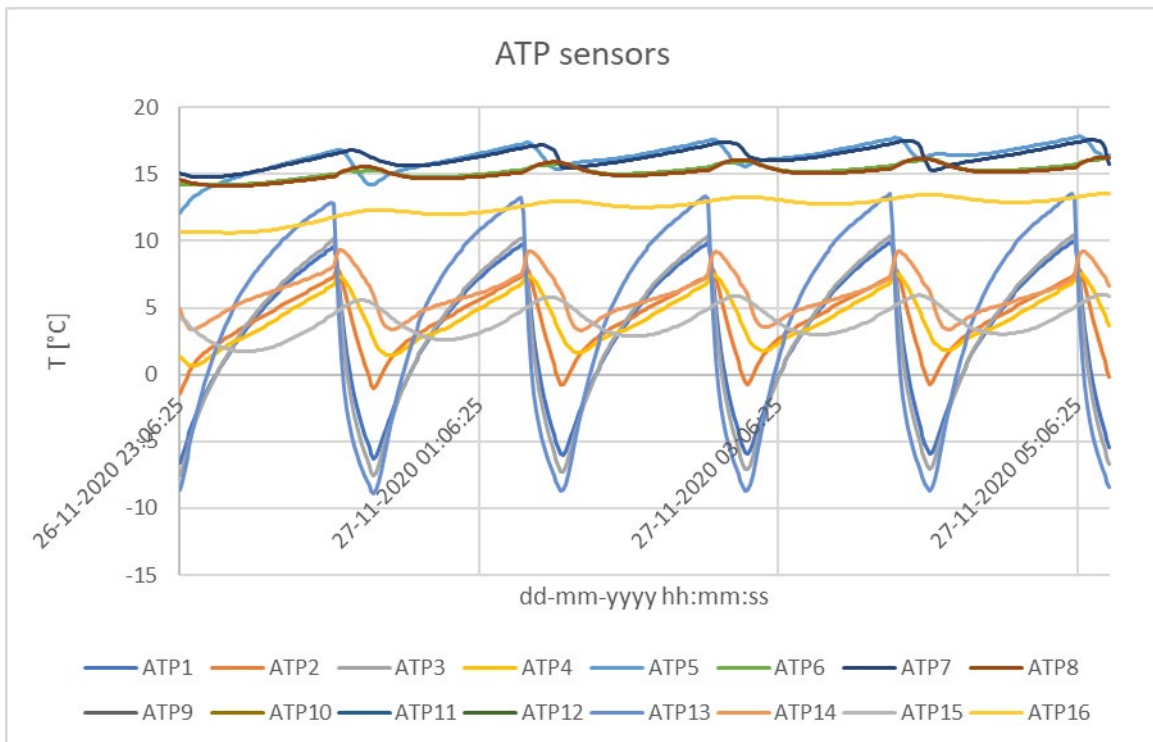


Figure 63 recorded steady state temperatures for test 39.

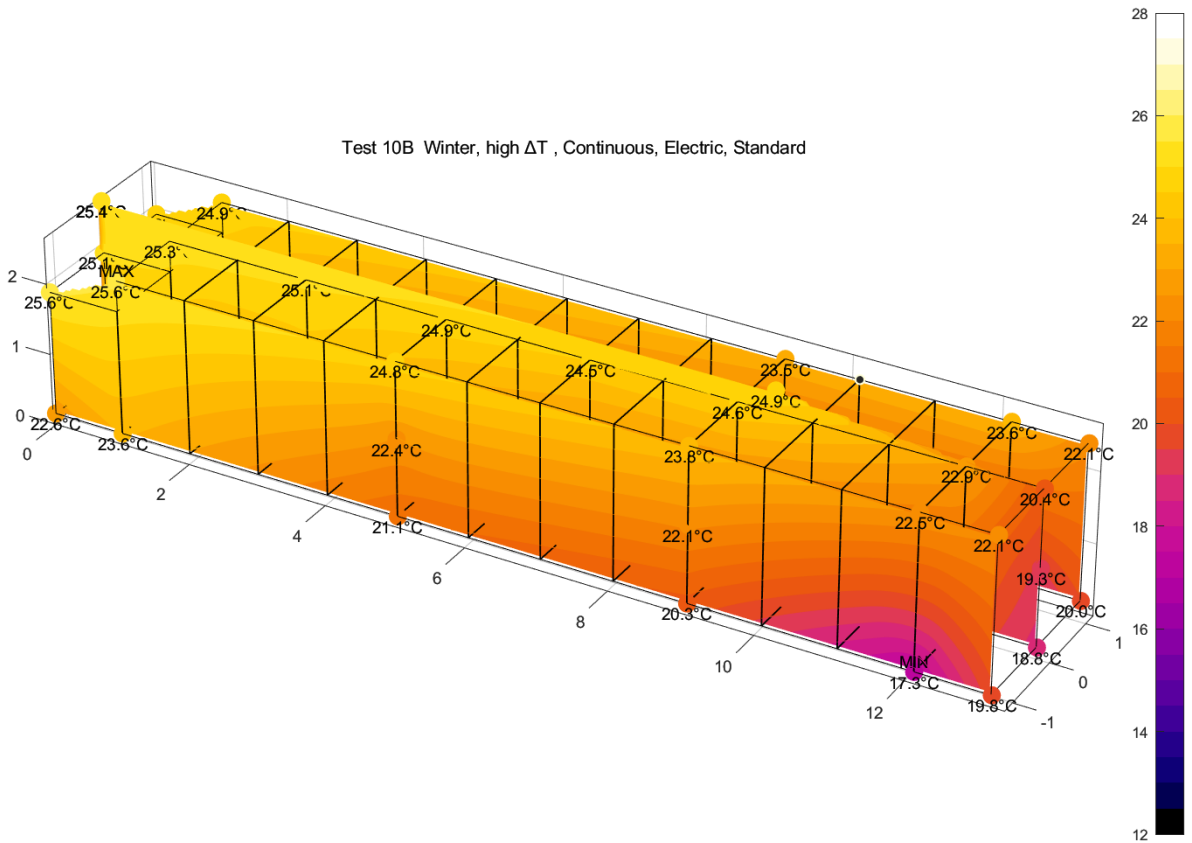


Figure 66 3D contour plots of steady state temperatures during test 10B.

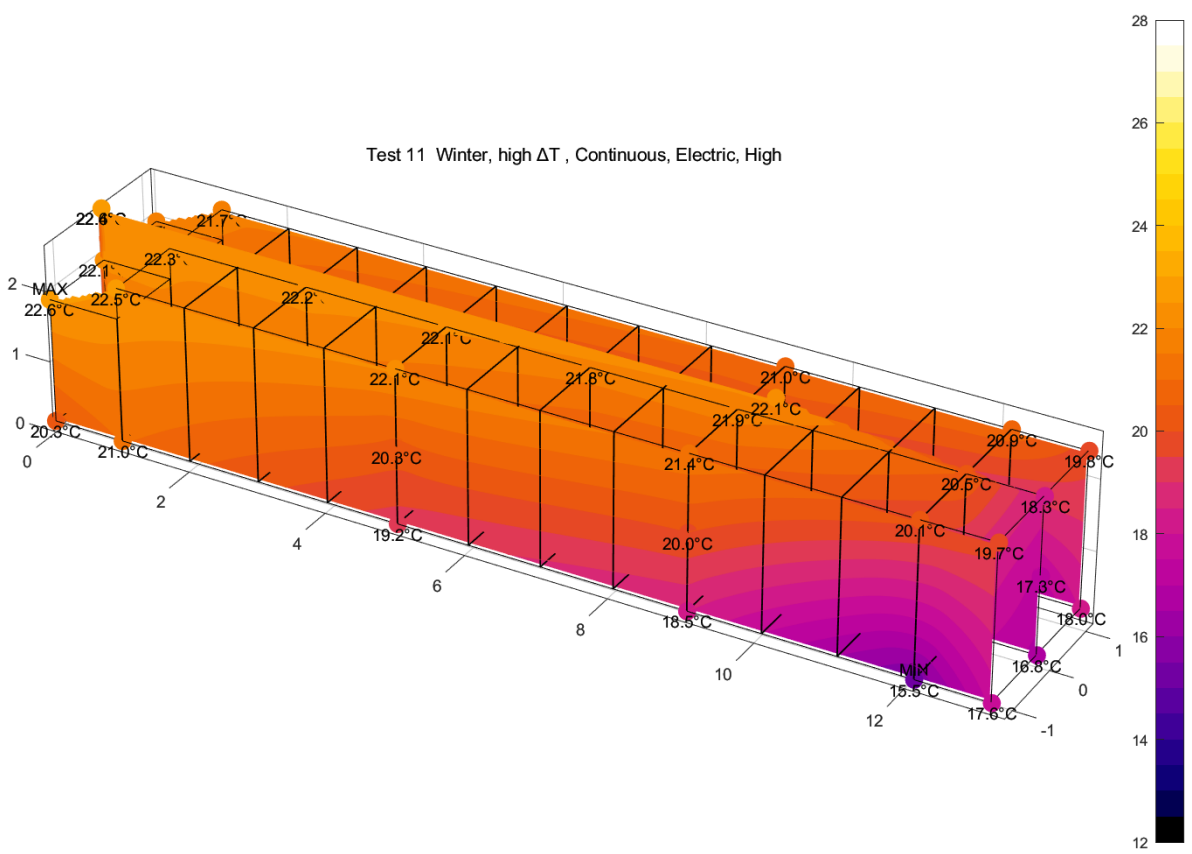


Figure 67 3D contour plots of steady state temperatures during test 11.

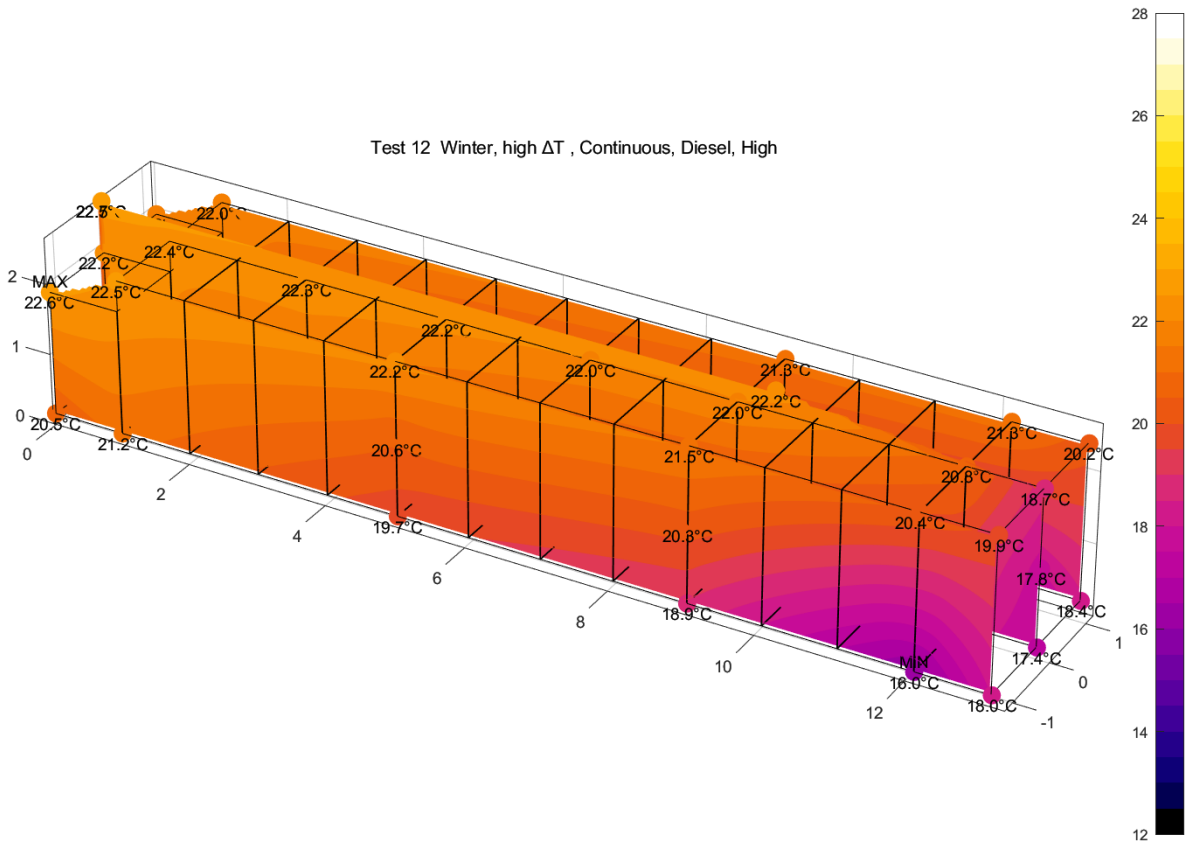


Figure 68 3D contour plots of steady state temperatures during test 12.

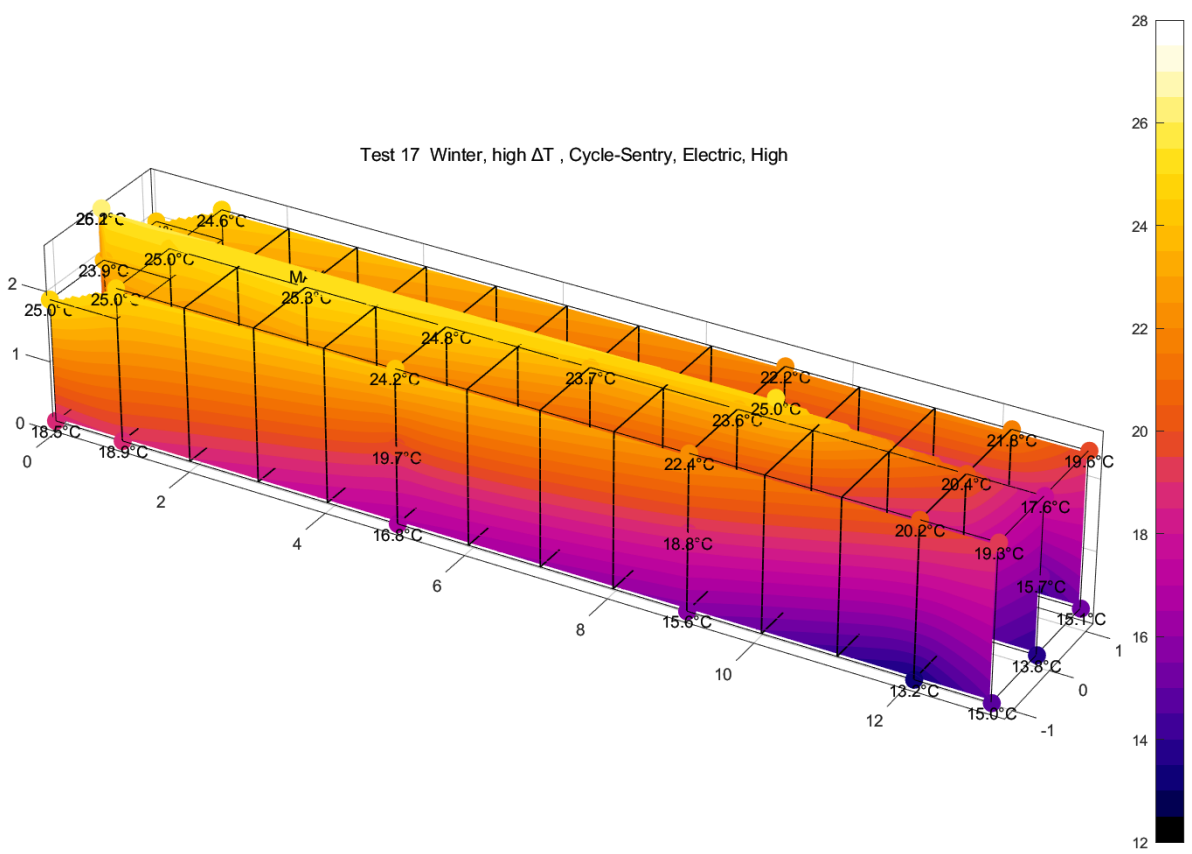


Figure 69 3D contour plots of steady state temperatures during test 17.

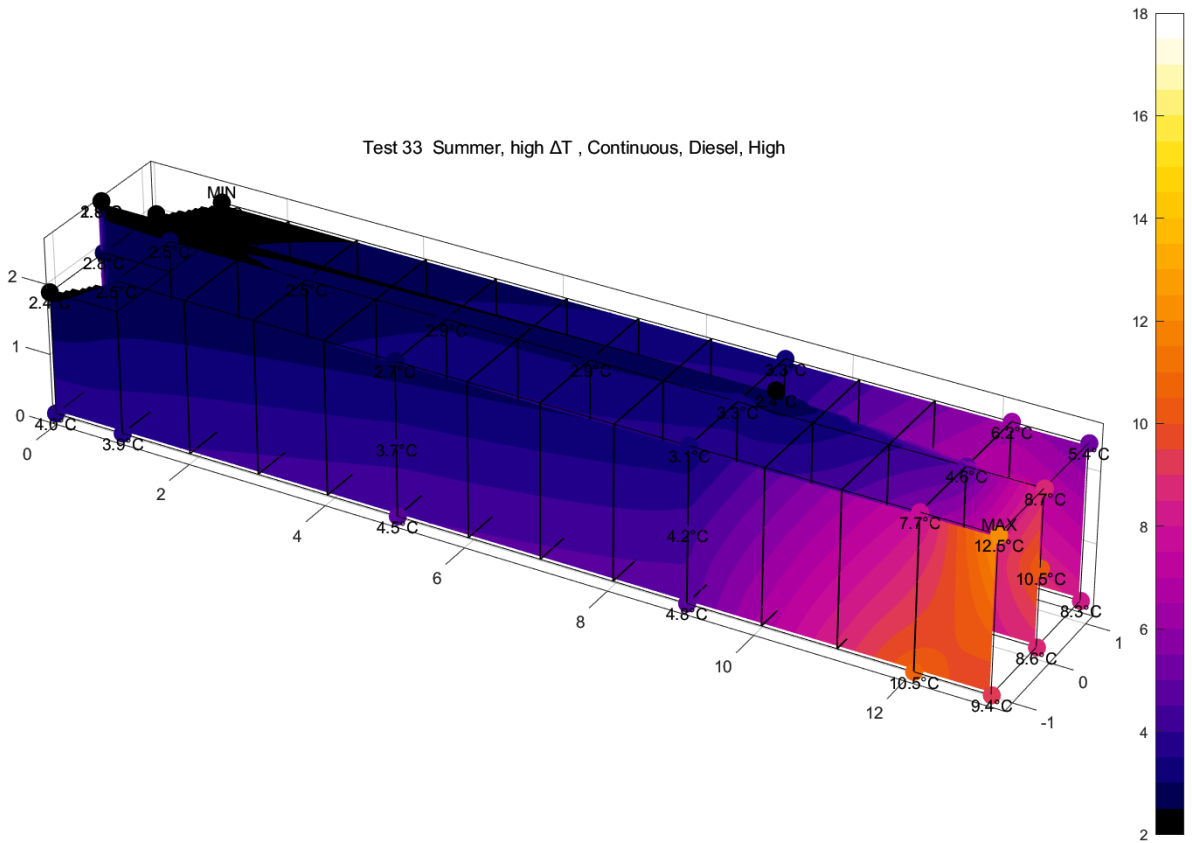


Figure 70 3D contour plots of steady state temperatures during test 33.

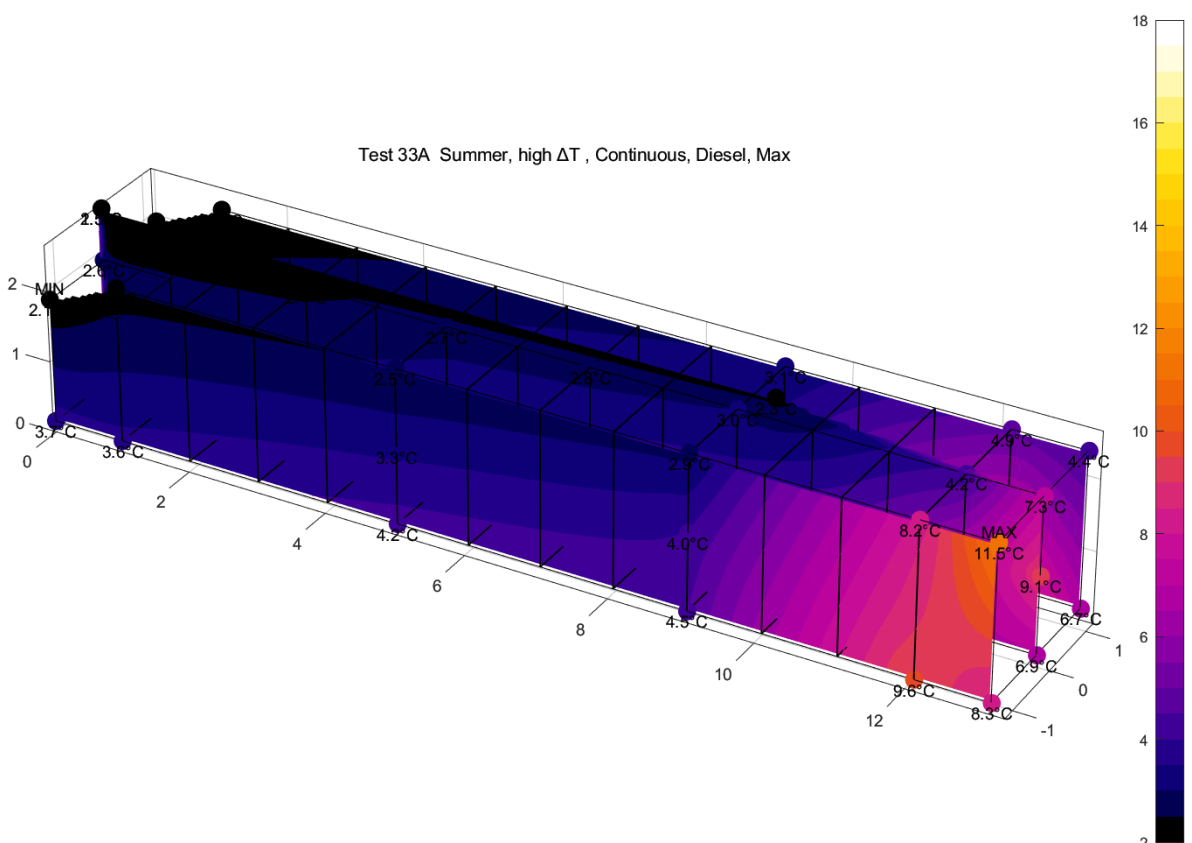


Figure 71 3D contour plots of steady state temperatures during test 33A.

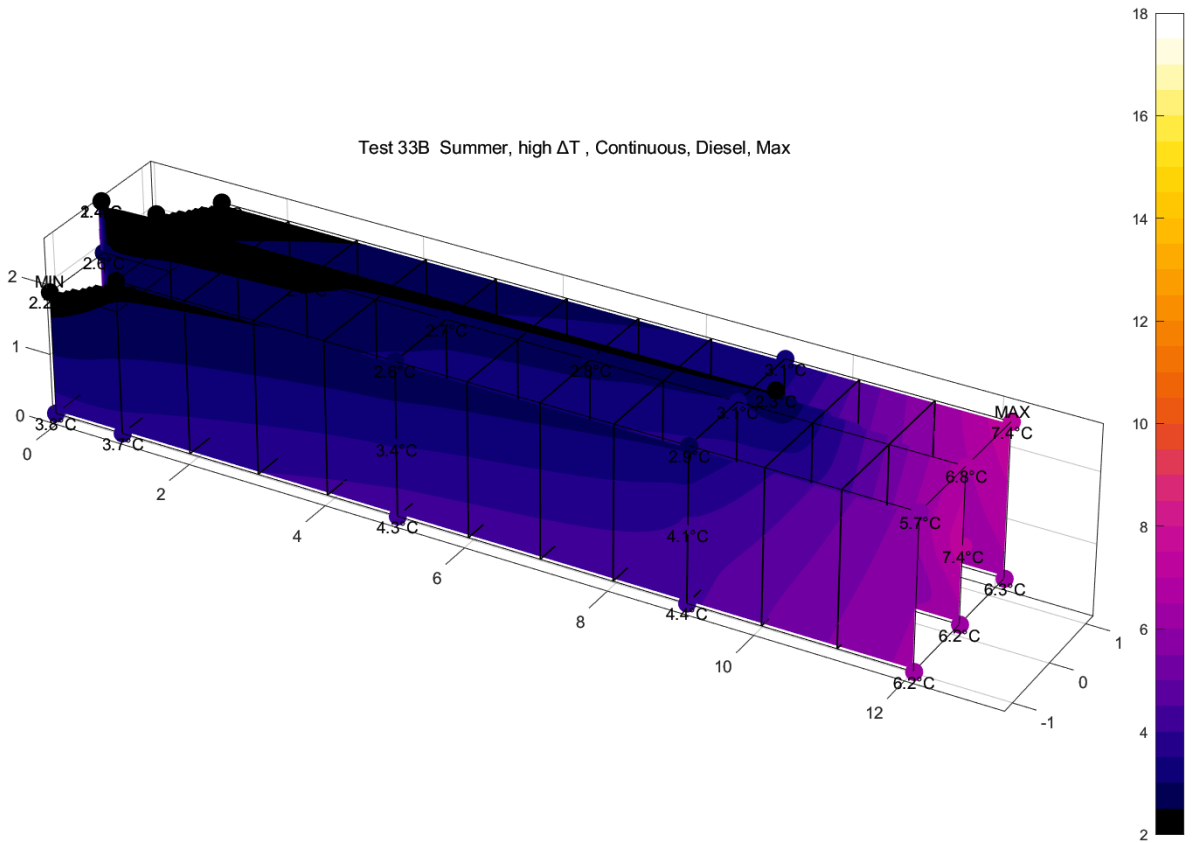


Figure 72 3D contour plots of steady state temperatures during test 33B.

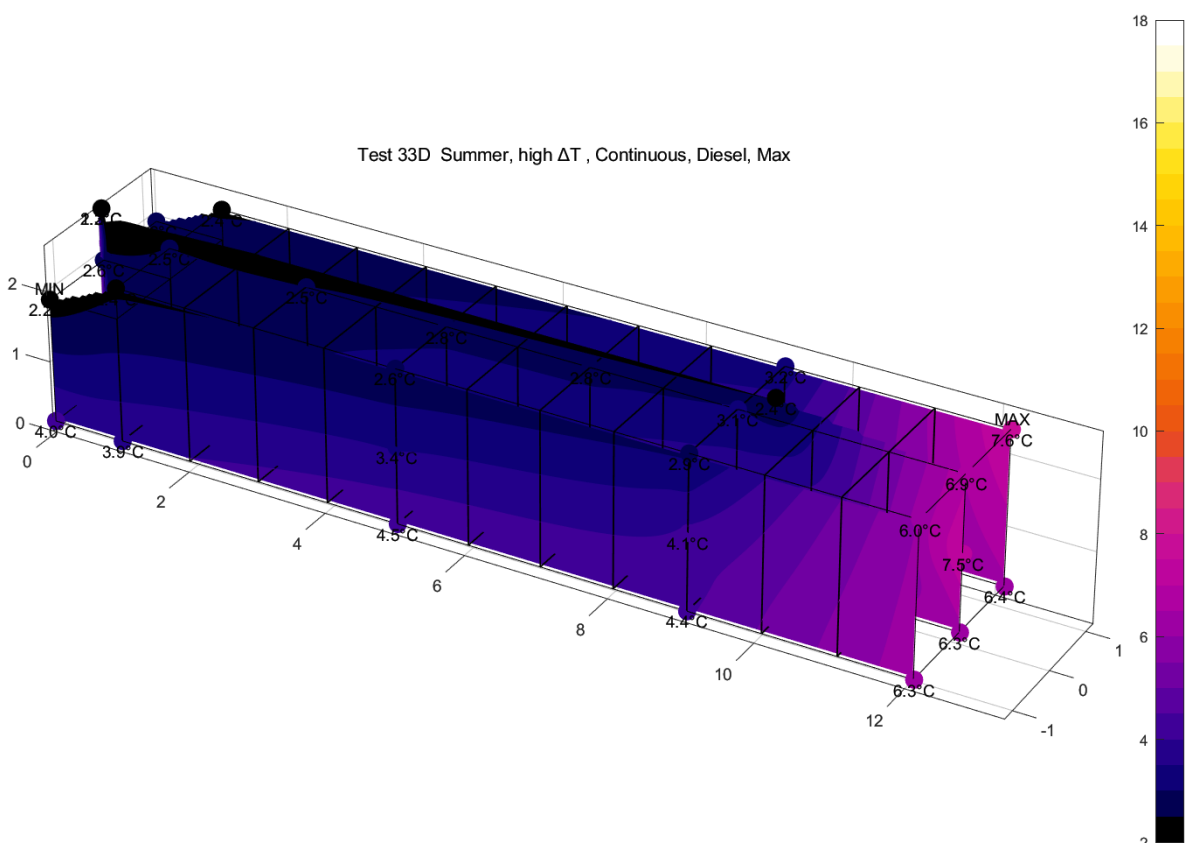


Figure 73 3D contour plots of steady state temperatures during test 33D.

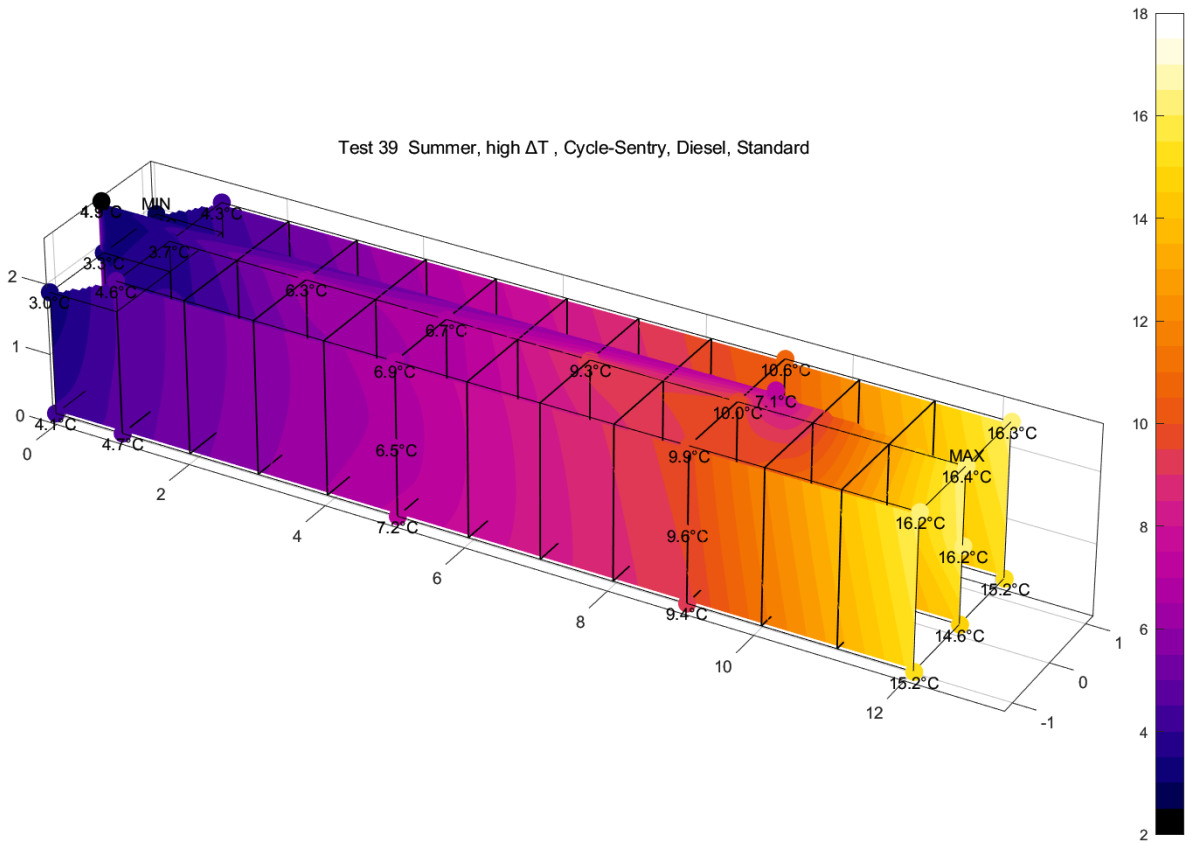


Figure 74 3D contour plots of steady state temperatures during test 39.

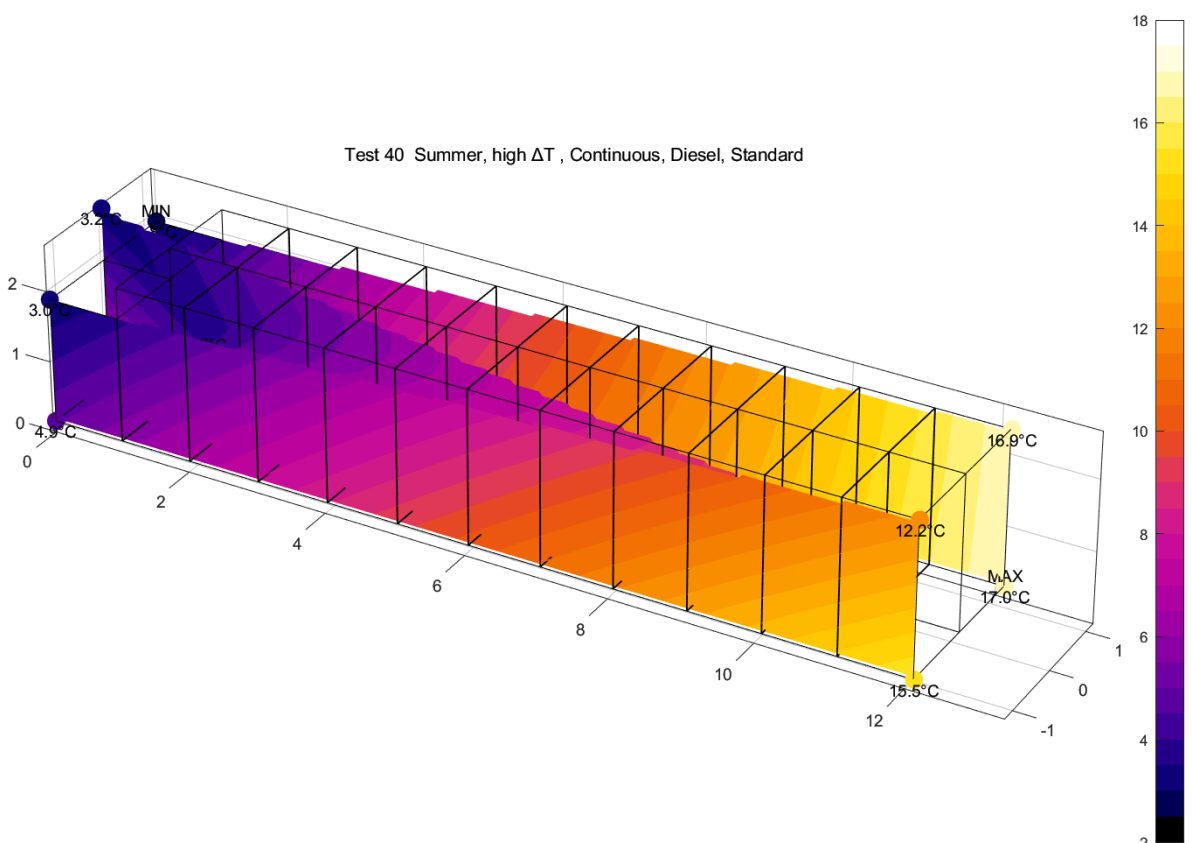


Figure 75 3D contour plots of steady state temperatures during test 40 (note the reduced number of sensors used in this interpolation).

Annex 3 Test log

date	Activity
23-10-2020	Container arrives
28-10-2020	Improvised return air duct completed
3-11-2020	Air velocities + Static pressure differences measured
6-11-2020 ~ 20-11-2020	Temperature mappings for configuration 1
20-11-2020 ~ 30-11-2020	Temperature mappings for configuration 2
9-12-2020 ~ 10-12-2020	K-value test
11-12-2020	Infrared photos of doors taken
11-12-2020	Measurement of supply air flow rate in empty container for multiple settings
15-12-2020	Container leaves

To explore
the potential
of nature to
improve the
quality of life



Wageningen Food & Biobased Research
Bornse Weilanden 9
6708 WG Wageningen
The Netherlands
www.wur.eu/wfbr
E info.wfbr@wur.nl

Report 2179

Confidential

The mission of Wageningen University & Research is "To explore the potential of nature to improve the quality of life". Under the banner Wageningen University & Research, Wageningen University and the specialised research institutes of the Wageningen Research Foundation have joined forces in contributing to finding solutions to important questions in the domain of healthy food and living environment. With its roughly 30 branches, 6,800 employees (6,000 fte) and 12,900 students, Wageningen University & Research is one of the leading organisations in its domain. The unique Wageningen approach lies in its integrated approach to issues and the collaboration between different disciplines.

